Manuscript version May 2nd, 2020

Parkinson Disease-Linked Parkin Mediates Redox Reactions That Lower Oxidative Stress In Mammalian Brain

Daniel N. El Kodsi[1,2]*, Jacqueline M. Tokarew[1,2]*, Rajib Sengupta[3,3^],
Nathalie A. Lengacher[1], Andy C. Ng[1], Heather Boston[1], Qiubo Jiang[1], Carina Palmberg[3],
Chantal Pileggi[4], Bojan Shutinoski[1], Juan Li[1], Angela P. Nguyen[1], Travis K. Fehr[1,2],
Doo Soon Im[2,2^], Steve Callaghan[2], David S. Park[2,2^], Matthew J. LaVoie[5],
Jennifer A. Chan[6,6^], Masashi Takanashi[7], Nobutaka Hattori[7], Rajiv R. Ratan[8],
Luigi Zecca[9], Lawrence Puente[10], Gary S. Shaw[11], Mary-Ellen Harper[4], Arne Holmgren[3%],
Julianna J. Tomlinson[1,12]#, and Michael G. Schlossmacher[1,2,12,13]#

[1]Program in Neuroscience, Ottawa Hospital Research Institute, Ottawa, ON, Canada

[2]Department of Cellular and Molecular Medicine ([2^]Present address: Hotchkiss Brain Institute, University of Calgary, Calgary, AB, Canada), and

[4]Department of Biochemistry, Microbiology and Immunology Faculty of Medicine, and Ottawa Institute of Systems Biology, University of Ottawa, Ottawa, ON, Canada

[3]Department of Biochemistry, Karolinska Institute, Stockholm, Sweden; [3^]Present Address: Amity Institute of Biotechnology, Amity University, Kolkata, West Bengal, India

[5]Ann Romney Center for Neurologic Diseases, and [6]Department of Pathology, Brigham and Women's Hospital, Boston, MA, USA; [6^]Present Address: Department of Pathology and Laboratory Medicine, University of Calgary, Calgary, AB, Canada

[7]Department of Neurology, Juntendo University School of Medicine, Tokyo, Japan

[8]Department of Neurology, Burke Rehabilitation Institute, Weill-Cornell College of Medicine, New York, NY, USA

[9]Institute of Medical Technologies, Italian National Research Council, Milan, Italy

[10]Proteomics Core Facility, Ottawa Hospital Research Institute, Ottawa, ON, Canada

[11]Department of Biochemistry, University of Western Ontario, London, ON, Canada

[12]University of Ottawa Brain and Mind Research Institute, Ottawa, ON, Canada

[13]Division of Neurology, Department of Medicine, The Ottawa Hospital, Ottawa, ON, Canada

*These authors contributed equally to this work; [%]deceased

#Lead contacts: jtomlins@uottawa.ca; mschlossmacher@ohri.ca

SUMMARY

We recently hypothesized that parkin plays a role in redox homeostasis and provided evidence that it directly reduces hydrogen peroxide (H_2O_2) *in vitro*. Here, we examined this anti-oxidant activity *in vivo*. Informed by findings in human brain, we demonstrate that elevated oxidative stress promotes parkin insolubility in mice. In normal mouse brain parkin was partially oxidized, *e.g.,* at cysteines 195 and 252, which was augmented by oxidative stress. Although under basal conditions H_2O_2 levels were unchanged in adult *prkn*$^{-/-}$ brain, a parkin-dependent reduction of cytosolic H_2O_2 was observed when mitochondria were impaired, either due to neurotoxicant exposure (MPTP) or *Sod2* haploinsufficiency. In accordance, markers of oxidative stress, *e.g.,* protein carbonylation and nitrotyrosination, were elevated in the cytosol but not in mitochondria from *prkn*$^{-/-}$ mice. Nevertheless, this rise in oxidative stress led to changes in mitochondrial enzyme activities and the metabolism of glutathione in cells and mammalian brain. In parkin's absence reduced glutathione concentrations were increased including in human cortex. This compensation was not due to new glutathione synthesis but attributed to elevated oxidized glutathione (GSSG)-reductase activity. Moreover, we discovered that parkin also recycled GSSG to its reduced form. With this reaction, parkin became S-glutathionylated*, e.g.,* at cysteines 59 and human-specific 95. This oxidative modification was reversed by glutaredoxin. Our results demonstrate that cytosolic parkin mediates anti-oxidant reactions including H_2O_2 reduction and glutathione regeneration. These reducing activities lead to a range of oxidative modifications in parkin itself. In parkin-deficient brain oxidative stress rises despite changes to maintain redox balance.

64 **INTRODUCTION**

65 Parkinson disease (PD) is a progressive, heterogeneous disorder of the human brain that
66 remains incurable. Young-onset, autosomal-recessive PD (ARPD) due to deficiency in
67 parkin (encoded by *PRKN*) is restricted to the degeneration of dopamine producing
68 neurons in the *S. nigra* and *L. coeruleus*[1]. In the ageing human brain, these neurons are
69 susceptible to degeneration because of unique features. These include: extensive
70 arborization; a high number of axonal mitochondria; the presence of metals in redox-
71 reactive forms[2]; ongoing generation of toxic dopamine metabolites in the cytosol; a
72 greater need to buffer Ca^{2+} ions; and collectively, a greater degree of oxidative stress[3-5].
73
74 Parkin is a RING-carrying protein with ubiquitin ligase activity that is involved in the
75 regulation of mitophagy and immune-related functions[6,7,8]. The role for each of these
76 functions in relation to ARPD development remains unknown. We recently described that
77 parkin itself is highly oxidized in human brain, and discovered that it acts as a redox
78 molecule to decrease dopamine metabolism-associated stress[9,10].
79
80 Oxidative stress and mitochondrial damage have been implicated in the pathogenesis of
81 several brain disorders including PD[11]. Mitochondrial dysfunction, as induced by the
82 neurotoxicants 1-methyl-4-phenyl-1,2,3,6-tetrahydropyridine (MPTP) and rotenone,
83 augments oxidative stress[12]. The integrity of the cellular thiol pool, a network formed by
84 glutathione and the cysteine proteome, is essential in maintaining redox homeostasis and
85 thus to the survival of long-lived neurons. The reduced form of glutathione (GSH) plays a
86 critical role as an anti-oxidant, as co-factor of enzymes, and as a reservoir of cellular
87 thiols. Accordingly, a decline in GSH has been implicated in many human disorders
88 including neurodegenerative diseases[13].
89
90 Genomic deficiency in parkin in mice does not induce loss of dopamine neurons, and
91 *prkn*$^{-/-}$ animals do not develop parkinsonism. However, unbiased studies have revealed
92 proteomic changes in these animals[14,15]. There, we noted that a majority of dysregulated
93 proteins in the brain, which showed altered isoelectric points on 2D-gels, had been
94 previously identified as enzymes (55/92; 59.8%). Many of the proteins were also known

95 as redox-sensitive proteins (72/92; 78.2%), *e.g.,* peroxiredoxins, glyoxalase and
96 aconitase-2[14,15]. These findings suggested to us that posttranslational modifications,
97 rather than changes in protein abundance, could have explained their dysregulation.
98
99 When taken together with previous reports of parkin's sensitivity to pro-oxidants[9,16], we
100 hypothesized that: one, thiol-rich parkin is altered in response to cellular redox changes;
101 two, parkin itself plays a role in lowering oxidative stress *in vivo,* thus influencing redox-
102 state and redox-sensitive enzymes; and three, the loss of parkin's anti-oxidant effects
103 contributes to mitochondrial changes. We therefore characterized parkin's redox activity
104 *in vitro*, explored the downstream oxidative changes in cells and mouse models with low
105 or absent parkin expression, and investigated parkin's effects on the thiol network. This
106 work was informed by parallel efforts, which focused on parkin's processing in human
107 midbrain and its role in dopamine metabolism[10].
108
109
110 **RESULTS**
111 **Mitochondrial and cytosolic stress conditions lead to oxidation of cellular parkin**
112 Using cell-based paradigms, we first analyzed parkin's response to cytosolic and
113 mitochondrial stressors. Chinese hamster ovary cells that stably express wild-type (WT)
114 human *PRKN* cDNA (CHO-parkin) and control cells, which in our hands showed little
115 endogenous parkin by routine Western blotting, were exposed to different levels of
116 hydrogen peroxide (H_2O_2, 0.2 or 2mM) or carbonyl-cyanide-m-chlorophenyl-hydrazine
117 (CCCP, 10μM). Under these stress conditions, which did not cause cell death, we
118 observed the time-dependent loss of parkin's monomer (~52.5 kDa) and an increase in
119 high molecular weight (HMW) species (**Fig. 1a**)[16]. These biochemical changes were seen
120 under non-reducing electrophoresis conditions and thus interpreted as involving parkin
121 thiol-based oxidation. Intriguingly, this oxidation was specific to parkin as endogenous,
122 redox-sensitive and ARPD-linked Dj-1[17] did not undergo such changes (**Fig. 1a**).
123
124 In oxidative stress-exposed, human embryonic kidney (HEK293) cells, which transiently
125 over-expressed *PRKN*, we also observed HMW smear formation. Parkin became

126 progressively gel excluded (aggregated) and insoluble following exposure to increasing
127 concentrations of H_2O_2 (**Fig. 1b**). Since these HMW forms of parkin were reversed with
128 dithiothreitol (DTT; **Extended Data Fig. 1a, c**), we postulated that these modifications
129 occurred due to increasing oxidation of parkin's cysteines[16]. We tested this using N-
130 ethylmaleimide (NEM) and iodoacetamide (IAA), which irreversibly alkylate free thiols.
131 There, we found that pre-incubation of cells with NEM or IAA blocked HMW smear
132 formation of parkin and preserved its solubility during H_2O_2 stress (**Fig. 1b; Extended**
133 **Data Fig. 1b**). Complementing these findings, we mapped several cysteines in
134 recombinant (r-) parkin, which became oxidized when the protein was subjected to rising
135 H_2O_2 levels *in vitro*, thereby promoting its aggregation and insolubility[10].
136
137 Intriguingly, exposure to DTT also lowered parkin solubility in cells (**Extended Data**
138 **Fig. 1c**), which suggested that parkin's structure is altered under excessive oxidizing and
139 excessive reducing conditions. These results demonstrated that human parkin undergoes
140 thiol chemistry-based changes in cells during redox stress.
141
142 **Excessive ROS exposure in mice promotes parkin insolubility**
143 Under stress-free conditions, parkin resides in the cytosol of cells (**Fig. 1a, b**) and rodent
144 brain[18,19]. In contrast, in human control brain parkin is largely insoluble after the 4th
145 decade of life[10,19]. To better understand the link between parkin's oxidation and
146 insolubility, we sought to validate these findings in mice in three different ways. First,
147 freshly dissected brains from WT mice were homogenized either in the presence or
148 absence of H_2O_2 to generate high amounts of reactive oxidative species (ROS). Lysates
149 were then fractionated and separated into soluble *vs.* insoluble fractions; in the latter,
150 proteins were extracted using 2-10% SDS. Exposure to H_2O_2 *in situ* led to a significant
151 loss in solubility of mouse parkin and recovery in the insoluble fraction ($P<0.001$), as
152 monitored by reducing SDS/PAGE. No such shift was seen for murine Dj-1 (**Fig. 1c, d**).
153
154 Secondly, we examined parkin's response to oxidative stress *in vivo.* We injected a single
155 dose of MPTP into the peritoneum of adult mice at a dose (40mg/kg) that induces
156 oxidative stress without neuronal death[20]. After one hour, brains were collected and

157 serially fractionated. The brief exposure to MPTP led to a decline of >50% in soluble
158 parkin when compared to saline-treated controls. As expected, parkin's detection rose in
159 the insoluble fraction ($P<0.05$; **Fig. 1e; Extended Data Fig. 1d, e**).
160
161 In a third approach, we tested whether a genetically induced, mitochondrial defect altered
162 parkin solubility. We chose *Sod2*$^{+/-}$ haploinsufficient mice with lower expression of
163 mitochondrial superoxide dismutase-2 (aka MnSOD). Reduced MnSOD2 activity
164 (**Extended Data Fig. 1h, i**) results in systemically elevated oxidative stress[21]. As
165 expected, parkin solubility had shifted in adult *Sod2*$^{+/-}$ brain ($P<0.05$; **Fig. 1f**; **Extended**
166 **Data Fig. 1j, k**). We concluded that toxicologically and genetically induced, oxidative
167 stress led to parkin insolubility in mammalian brain. We postulated that this change
168 corresponded with fewer free thiols, due to increasing oxidation, within parkin itself.
169
170 **Exposure to MPTP increases parkin oxidation in the brain**

171 To test this, we employed liquid chromatography and mass spectrometry (LC-MS/MS).
172 Brains from mice injected with MPTP or saline (as above) were homogenized in the
173 presence of IAA to alkylate free cysteines and prevent thiol oxidation during processing.
174 Parkin-enriched isolates were separated by SDS/PAGE (**Extended Data Fig. 1f**).
175 Monomeric, alkylated parkin was gel-excised, trypsin digested and subjected to LC-
176 MS/MS. We recorded a <20% decline in the relative amount of unmodified cysteines in
177 parkin peptides from MPTP-treated mice compared to those from saline-injected controls
178 (**Extended Data Table 1**). Furthermore, we found that several cysteines had been
179 oxidized under normal conditions*, e.g.,* to dehydroalanine, sulfinic acid and sulfonic acid
180 (**Extended Data Table 1**). Intriguingly, residues C195 and C252 were frequently
181 identified as irreversibly oxidized in mouse brain (**Extended Data Table 1; Extended**
182 **Data Fig. 1g**). In parallel studies of human parkin, we found that the oxidation of
183 orthologous cysteines*, e.g.,* C253, contributed to its progressive insolubility[10].
184
185 **Parkin reduces hydrogen peroxide to water in a thiol-dependent manner**
186 We recently provided evidence that WT r-parkin reduced H_2O_2 to water *in vitro* by
187 reciprocal oxidation of its thiol groups[10]; ARPD-linked point mutants did so less well.

188 Here, we further explored the biochemical mechanisms underlying this activity. Human
189 r-parkin was nearly 5-fold more effective in lowering H_2O_2 levels than GSH at equimolar
190 concentrations, but was less potent than catalase (**Extended Data Fig. 2a)**. This
191 suggested that parkin shared a thiol-based activity with GSH. We confirmed this by
192 demonstrating that r-parkin's ability to reduce H_2O_2 was abrogated when its thiols were
193 either oxidized prior to the reaction or irreversibly blocked by NEM (**Extended Data**
194 **Fig. 2b, c**). Parkin did not exhibit peroxidase-type anti-oxidant activity (**Supp. Fig. 2D**).
195
196 Two other PD-linked proteins*, e.g.,* α-synuclein and DJ-1 (with 0 and 3 cysteines,
197 respectively; **Extended Data Fig. 2e**), had no detectable H_2O_2-lowering activity (**Fig.**
198 **2a**). Bovine serum albumin with the same number of cysteines as human parkin (n, 35)
199 and two RING-carrying E3 ubiquitin ligases, *e.g.,* RNF43 and HOIP (**Extended Data**
200 **Fig. 2e, f**), also failed to lower H_2O_2 (**Fig. 2a**). The latter results suggested that parkin's
201 structure played a role in its activity, which was not solely due to the presence of its four
202 RING domains, each of which chelates two Zn^{2+} ions (**Extended Data Fig. 1g**)[22].
203 Nevertheless, competitive chelation of Zn^{2+} ions by rising EDTA concentrations prior to
204 the reaction diminished r-parkin's antioxidant activity. This was partially, but not
205 completely, reversed when excess Zn^{2+} was added back to the reaction mix (**Extended**
206 **Data Fig. 2g**). Of note, EDTA and NEM alone had no effect on the assay (**Extended**
207 **Data Fig. 2h**). We concluded from these findings that parkin's H_2O_2-reducing activity
208 was: not enzymatic, required integrity of its tertiary structure, depended on free thiols,
209 and resembled GSH's mechanism of action.
210
211 ***PRKN* expression lowers hydrogen peroxide concentrations in the cytosol**
212 We next asked whether parkin contributed to redox balance in cells and *in vivo*. Under
213 basal conditions, HEK293-parkin cell lysates showed a trend toward lower levels of H_2O_2
214 when compared to controls; the difference became significant when we monitored intact
215 cells (**Fig. 2b**; **Extended Data Fig. 2i**). When HEK293 cultures were exposed to rising
216 oxidative stress, *e.g.,* after CCCP treatment or excessive levels of H_2O_2 in the presence of
217 aminotriazole (AT, a catalase inhibitor; **Extended Data Fig. 2a**), parkin-expressing cell
218 lysates showed a significantly lower level of ROS ($P<0.0001$; **Fig. 2b**).

219

220 We next tested parkin's effects on H_2O_2 concentrations in mouse brain using a validated
221 AmplexRed assay (**Extended Data Fig. 2j**). We found that basal ROS concentrations did
222 not differ between adult *prkn*$^{-/-}$ and WT mice, neither in the cytosol nor in isolated
223 mitochondria (**Fig. 2c,d; Extended Data Fig. 3b**). In contrast, exposure to MPTP caused
224 a significant elevation in endogenous ROS levels in parkin-deficient mice (P<0.001; **Fig.**
225 **2e**). Under basal conditions H_2O_2 levels were also higher in the cytosol of *Sod2*$^{+/-}$ mutant
226 and bigenic animals (*prkn*$^{-/-}$*//Sod2*$^{+/-}$), which we had created to further augment metabolic
227 stress (P<0.05; **Fig. 2c**; **Extended Data Fig. 1h, i**). Of note, at this age *Sod2*$^{+/-}$ and
228 bigenic mice did not show detectable cell loss (not shown). Unexpectedly, ROS levels
229 remained the same in isolated brain mitochondria from *Sod2*$^{+/-}$ mice (**Fig. 2d**), which
230 suggested rapid shuttling of superoxide from their mitochondria into the cytosol[23].
231

232 ***Prkn* gene expression lowers oxidative stress in mammalian brain**

233 We next examined the degree of protein carbonylation, a marker of chronically elevated
234 H_2O_2, in the same mouse lines. Carbonyl content was increased in the cytosol of *prkn*-
235 mutant brain, even under basal conditions, consistent with a previous report by Palacino
236 et al., who had used a different mouse model[14], but remained normal in isolated
237 mitochondria. There, we also observed a *prkn*-null allele dosage effect (**Fig. 2f**). As
238 expected, carbonyl content was further increased in the bigenic mice when compared to
239 WT, *prkn*$^{-/-}$ and *Sod2*$^{+/-}$ littermates (P<0.001 and P<0.05 respectively; **Fig. 2g**). A second
240 marker of oxidative stress-induced protein modification, *i.e.,* nitrotyrosination, was also
241 increased in the cytosol of *prkn*$^{-/-}$ mice including in the heart (**Extended Data Fig. 3c, d**).
242

243 We next examined protein carbonyl content in patients with *PRKN*-linked ARPD and
244 control subjects (each, n=4). These had been matched for age, *post mortem* interval,
245 ethnicity and hospital morgue (**Extended Data Fig. 3a**)[24]. In the absence of human
246 parkin, protein carbonyl levels showed a trend toward elevation. Cortices from three,
247 non-*PRKN*-linked parkinsonism cases revealed the same degree of carbonyl content as
248 age-matched controls (**Fig. 2h**). Using a linear regression model with the protein carbonyl
249 content measured in all brains (mouse and human) as the dependent variable, we found

250 that oxidative stress correlated with parkin deficiency; the co-efficient was -0.3754 (95%
251 CI, -0.6611–0.0053; P=0.05; **Fig. 2i**). Of note, in these redox studies, we did not observe
252 any sex effect. Together, these results established that WT parkin contributed to H_2O_2
253 reduction in cells and brain during basal activities and with rising oxidative stress.
254
255 ***Prkn* gene expression affects redox-dependent enzymatic activity**
256 To link these findings back to proteomic changes downstream of parkin deficiency, we
257 explored redox-dependent enzymatic activities. In the brains of *prkn* $^{-/-}$ mice, we found
258 significantly increased activity of aconitase-2 (Aco2), a $NADP^+$-linked enzyme, under
259 basal conditions when compared to littermates (P<0.001; **Fig. 2j**). Following exposure of
260 isolated brain mitochondria to H_2O_2, Aco2 and creatine kinase (mtCK) activities were
261 decreased in both WT and *prkn*-null brains, as expected; however, their activities
262 remained measurably higher in *prkn*$^{-/-}$ mitochondria (P<0.05 and P<0.01, respectively;
263 **Fig. 2j**; **Extended Data Fig. 3e**). Importantly, the levels of detectable murine and human
264 Aco2 and mtCK proteins were not altered in these brains, neither in whole lysates nor in
265 isolated mitochondria, when comparing WT *vs*. mutant *PRKN* genotypes (**Extended**
266 **Data Fig. 3b, f-h**). Although increased cytosolic ROS production in parkin-deficient
267 brain could have led to the proteomic changes detected in these animals, this would not
268 have fully explained altered enzyme activities by Aco2 and mtCK under redox stress. We
269 suspected that other redox effects in *prkn*$^{-/-}$ mice, such as changes in the thiol network,
270 contributed to these results.
271
272 **Parkin contributes to the thiol network during oxidative stress**
273 To test whether parkin expression contributed to the thiol network, we first compared
274 survival rates of CHO-parkin cells following exposure to H_2O_2 after depletion of GSH
275 with buthionine sulfoximine (BSO). Treatment with either H_2O_2 (1h) or BSO alone
276 (48hs) did not cause cell death (**Extended Data Fig. 2k**). Under combined stress
277 conditions, *PRKN* expression was protective: it led to significantly less cell death
278 (P<0.05; **Fig. 3a**) and normalized ROS levels (P<0.001; **Fig. 3b**), resulting in reciprocal
279 parkin oxidation (Fig. 1A). Treatment with excess n-acetylcysteine, an abundant source
280 of free thiols, resulted in similarly protective effects as did *PRKN* expression (**Fig. 3a, b**).

281 Based on these results, we conjectured that parkin supplements the cellular thiol network
282 through its own free thiols, which could neutralize ROS.
283
284 ***PRKN* gene expression alters glutathione redox state in cells and human brain**
285 We examined this by directly measuring levels of GSH (reduced) and GSSG (oxidized)
286 by HPLC. There, CHO-control cells had relatively high concentrations of GSH and low
287 amounts of GSSG, with an elevated ratio of GSH:GSSG (**Fig. 3c**). Increased expression
288 of WT parkin significantly reversed these redox indices ($P<0.01$ and $P<0.001$), but no
289 change was found in the total concentration of GSH and GSSG (**Extended Data Fig. 4a**).
290 Consistent with reports of CHO cells displaying high stress tolerance[25], exogenously
291 added H_2O_2 did not substantially change the redox indices between CHO-control and
292 CHO-parkin cells with the exception of now equalized GSSG levels (**Fig. 3d**). Parkin-
293 dependent changes in GSH levels and GSH:GSSG ratios were also observed in
294 transfected HEK293 cells (not shown) and human, dopamine SH-SY5Y cells (**Fig. 3e**).
295
296 The interplay between *PRKN* expression and GSH redox state was further validated in
297 human brain using cortex specimens from patients with *PRKN*-linked ARPD and healthy
298 controls (as used above). In the absence of detectable parkin, reduced GSH levels as well
299 as the ratio of GSH:GSSG were significantly increased ($P<0.01$ and $P<0.05$ respectively).
300 No differences were seen for GSSG levels (**Fig. 3f**) or the total concentration of GSH and
301 GSSG (**Extended Data Fig. 4b**). Intriguingly, the redox changes recorded in human
302 brain closely mirrored those in CHO cells exposed to oxidative stress (**Fig. 3d**). We
303 concluded that a reciprocal relationship existed between *PRKN* expression and GSH
304 levels *in vivo*. When combining these results and using a linear regression model with
305 GSH levels as the dependent variable, we found that lower expression of parkin was
306 associated with higher GSH levels; the co-efficient was -0.6889 (95% CI, -0.849 to -
307 0.411; $P<0.0001$; **Fig. 3g**).
308
309 ***Prkn* deletion alters glutathione metabolism in mice with a mitochondrial defect**
310 Two groups previously reported elevated GSH levels in *prkn* $^{-/-}$ mice and their glia[26,27].
311 When examining the same colony generated by Itier et al. using our HPLC method,

312 parkin-deficient brains showed similar but non-significant trends for thiol changes, *i.e.*
313 higher concentrations of reduced GSH, lower levels of GSSG, and a higher GSH:GSSG
314 ratio (**Fig. 3h**). Brains from *Sod2*$^{+/-}$ haploinsufficient animals showed identical results.
315 When endogenous oxidative stress was further elevated in bigenic (*prkn* $^{-/-}$*//Sod2*$^{+/-}$)
316 animals, the same changes in redox indices were detected (P<0.05; **Fig. 3h**), as measured
317 in human parkin-deficient cells and cortices (above). These results established a relation
318 between parkin protein expression, glutathione redox state and degree of oxidative stress
319 *in vivo*. We next studied potential mechanism(s) to explain it.
320
321 ***De novo* synthesis of glutathione is not altered in parkin-deficient brain**
322 We first examined GSH *de novo* synthesis. When we measured the total pool of
323 glutathione (GSH and GSSG) by HPLC in our parkin-deficient *vs.* WT parkin expression
324 paradigms, we saw no differences for the total concentration across cell cultures, murine
325 brains and human cortices (**Extended Data Fig. 4a, b, c**). In accordance, we found no
326 difference in transcript numbers for the two rate-limiting enzymes in GSH synthesis, *i.e.,*
327 the glutamate-cysteine-ligase-catalytic (*GCLC*) and glutamate-cysteine-ligase-modifier
328 (*GCLM*) subunits[28], or for *Dj-1,* in these mouse lines (**Extended Data Fig. 4d, e**).
329 Unexpectedly, in bigenic mice, where we did record a significant rise in the total
330 glutathione (GSH + GSSG) concentration (P<0.05), we found no higher copy numbers
331 for *GCLC* or *GCLM* mRNA (**Extended Data Fig. 4c,e**). Thus, *de novo* synthesis from
332 transcription did not explain the glutathione redox changes seen in parkin's absence.
333
334 **Glutathione recycling is altered in *prkn*-null brain**
335 We next explored a second mechanism, namely enhanced regeneration of GSH by
336 glutathione reductase (GR). This enzyme is activated by rising levels of ROS or its
337 substrate (GSSG), and is inhibited by excess product levels, such as GSH or $NADP^+$ [29-31].
338 By using the Tietze method, which utilizes exogenous GR activity to indirectly measure
339 GSH and GSSG levels, we reproduced the same significant changes, *i.e.,* GSH elevation
340 (P<0.01), GSSG lowering (P<0.01) and the rise of the GSH:GSSG ratio, in *prkn* $^{-/-}$ mice
341 as found in cells and human brain (**Fig. 4a** and **Fig. 3c-f**, respectively). These findings in
342 mouse brain matched the published results by Itier et al.; they suggested that GR activity

343 was indeed higher in parkin's absence. We reasoned that activation of endogenous GR
344 was even more elevated in ARPD cortices than in *prkn*$^{-/-}$ brain, because GSH levels were
345 higher in the former than the latter using the GR-independent HPLC method (**Fig. 3f-h**).
346

347 **Parkin contributes to the pool of recycled glutathione**

348 Based on the dynamic changes observed in the redox state of cells and tissues, we also
349 asked whether parkin had any direct effects on thiol network changes, such as via GSH
350 recycling. We specifically asked whether parkin interacted with GSSG. We first tested
351 this *in vitro* using recombinant proteins, both tagged and untagged, and eosin-labelled
352 GSSG (referred to as Di-E-GSSG) (**Extended Data Figs. 2f, 4f**). We discovered that full-
353 length, human parkin had concentration-dependent activity in reducing Di-E-GSSG to the
354 fluorescence-emitting E-GSH (545 nm) (**Fig. 4b**). Of note, Di-E-GSSG itself is non-
355 fluorescent due to quenching[32]. N-terminally truncated parkin comprising the IBR-
356 RING2 domains (aa 327-465) and a C-terminal RING2 peptide (aa 425-465) also showed
357 E-GSH-regenerating activity (**Extended Data Fig. 4f, g**; and not shown). In contrast, the
358 control protein-tag alone (*e.g.,* maltose-binding protein (MBP); ~50 kDa) and incubation
359 with E-GSH (without any Di-E-GSSG present) showed no activity in this assay (**Fig. 4b**).

360 Resulting from this biochemical reaction, the formation of E-S-glutathionylated parkin
361 (referred to as parkin-SG-E) was confirmed by using MBP-tagged parkin proteins, non-
362 reducing SDS/PAGE analyses and UV light. We found that the ~90 kDa MBP-parkin-
363 SG-E and the ~60 kDa MBP-IBR-RING2-SG-E proteins were only visible under UV
364 light after the incubation of native proteins with Di-E-GSSG (*e.g.,* **Extended Data Fig.
365 4gh**, lane 2 of left panel). Furthermore, the incubation of MBP-IBR-RING2-SG-E and
366 MBP-parkin-SG-E with either DTT or a reconstituted glutaredoxin-1 or -2 (Grx1, Grx2)
367 system[32] reversed the S-glutathionylation of parkin, confirming that oxidation in the form
368 of disulphide-bond formation had occurred during the earlier reaction (**Extended Data
369 Fig. 4h**). In accordance, parkin proteins without any -SG-E modification did not interact
370 with Grx1, Grx2, or thioredoxin-1 (Trx1; not shown). We reasoned that parkin's ability to
371 directly interact with GSSG could therefore alter the redox index of the GSH:GSSG ratio.

372 To test this, we incubated untagged r-parkin (1μM) with eosin-free ratios of
373 [GSH]:[GSSG] at a total concentration of 10μM per well (**Fig. 4c**). After 15 min, we
374 measured GSH concentrations with a specific assay. Following its incubation with GSSG
375 alone, we determined that under these conditions parkin was able to reduce up to 5
376 equivalents of GSSG to GSH (6.8μM GSH minus a baseline signal of 1.3μM for r-parkin
377 alone; **Fig. 4c**). Other ratios of [GSH]:[GSSG] showed analogous changes. Therefore, for
378 every recycled GSSG molecule one reduced GSH and one S-glutathionylated form
379 attached to parkin had been generated. These findings demonstrated a direct biochemical
380 effect by parkin onto its surrounding thiol network.

381 We next sought to map specific S-glutathionylation sites on parkin using MBP-parkin-SG
382 preparations by mass spectrometry, which was performed under non-reducing conditions.
383 Full-length MBP-parkin-SG-E was subjected to trypsin digestion followed by LC-
384 MS/MS and MALDI analyses. We detected two residues that were consistently S-
385 glutathionylated, *i.e.,* the conserved cysteine 59 and human-specific cysteine 95; each
386 carried an extra mass of 305.0682 (**Fig. 4d, e**), corresponding to S-linked glutathionylated
387 oxidation. A third, but less frequently identified residue to be S-glutathionylated was
388 cysteine 377 within parkin's IBR domain. To date, we have not yet identified modified
389 cysteine(s) in the C-terminal RING2 peptide, which also had shown GSSG-recycling
390 activity. We concluded from these results that S-glutathionylation represents a *bona fide*
391 oxidative modification of human parkin, which arises from its interaction with GSSG.
392
393
394 **DISCUSSION**
395 Our study generated four novel insights into the protective effects of PD-linked parkin:
396 One, we restaged in cell models and mouse brain the age-associated loss of parkin
397 solubility that occurs in human brain[10,19] by inducing its progressive oxidation using
398 mitochondrial and cytosolic stressors (**Fig. 1; Extended Data Fig. 1**). We then monitored
399 for specific cysteine oxidation sites in murine parkin using LC-MS/MS (**Extended Data**
400 **Fig. 2f, g; Extended Data Table 1**). There, we found a relative loss of free thiols in
401 parkin associated with the rise of oxidative stress in MPTP-treated mice. We also mapped

402 several cysteines that had undergone irreversible oxidation, such as to sulfinic and
403 sulfonic acid, under both basal and oxidizing conditions, *e.g.,* C211, C195, C237, C252,
404 and C376 (**Extended Data Table 1**). We noticed with interest –given the role of parkin's
405 phosphorylation by ARPD-linked PINK1 during mitophagy[33]- that S77 of murine parkin
406 was found phosphorylated in MPTP-exposed brain (**Extended Data Table 1**).
407
408 Two, we established that *PRKN* expression contributes to cytosolic ROS neutralization
409 and *in vivo* redox homeostasis; this, to limit oxidative stress in high energy-demanding
410 organs, such as the brain and heart. Its function in ROS neutralization complements
411 parkin's role in dopamine radicals-induced stress[10]. These anti-oxidant effects are
412 mediated by parkin's cysteines, which are sensitive to oxidizing as well as reducing
413 environments (**Fig. 2a; Extended Data Fig.2a-g**). We found that parkin contributes to
414 redox homeostasis downstream of oxidative stress production, as seen in lower carbonyl
415 contents of mouse and human tissues (**Fig. 2f-i**), as first described by Palacino et al.[14].
416 We also provided evidence that parkin's modulation of cytosolic ROS is linked to the
417 activities of redox-sensitive, mitochondrial enzymes (*e.g.,* Aco2; **Fig. 2j**), which were
418 previously found structurally altered (but mechanistically never explained) in parkin-
419 deficient mice[15]. Linking parkin's role in mitigating ROS concentrations in the cytosol to
420 changes in mitochondrial activity also helps explain the observation made by Berger et
421 al., who had postulated an 'intrinsic, pro-mitochondrial effect by cytosolic parkin'[34]. We
422 suspect that the structural changes in redox-sensitive proteins from *prkn*$^{-/-}$ mice[14,15] were
423 mediated by the net reduction in protein-based free thiols, thereby not only conferring
424 less protection from endogenously generated oxidative radicals (**Figs. 2, 3)**, but also
425 altering overall redox balance (including of co-factors) within the cell. Our results
426 therefore link parkin's own oxidation to concrete redox benefits in cells and organs, thus
427 explaining mechanistically why parkin functions as a 'multipotent, protective protein'[35].
428
429 Three, parkin's cellular protection from ROS appeared independent of E3 ligase activity.
430 Its oxidation had previously been widely interpreted as a loss of its function[36,37], Here, we
431 demonstrated that parkin confers cellular protection and ROS mitigation under oxidizing
432 conditions that would abrogate its E3 ligase activity[9]. We also determined that HMW

433 forms of parkin, which were produced during oxidizing conditions, collapsed when
434 exposed to DTT; this reversal would not occur for parkin species formed by auto-
435 polyubiquitination[38]. Our findings could suggest that E3 ligase function is not essential to
436 parkin's oxidative stress-mitigating role. However, parkin's redox-regulating activity
437 may not be mutually exclusive from its E3 ligase function. It is known that low levels of
438 oxidation can activate E3 ligase activity *ex vivo*; moreover, both cellular redox-regulation
439 and E3 ligase function are thiol-based[9,36,39,40]. In support of such a low level of parkin
440 activation, we noted that the protein is oxidized under basal conditions in both murine
441 (**Extended Data Table 1**) and human brain[10]. Furthermore, the reversible nature of some
442 (but not all) of these oxidative modifications suggests that parkin continuously undergoes
443 oxidative events *in vivo*. Therefore, we propose that distinct cellular conditions may
444 require more of parkin's redox functions, such as during elevated oxidative stress,
445 whereas others may demand more E3 activity, such as during organelle-specific
446 autophagy. Because powerful oxidative stressors are required to recapitulate -in mice-
447 parkin's aggregation and insolubility (**Fig. 1**), which occurs physiologically during
448 human brain ageing[10], we speculate that parkin is exposed to significantly higher
449 oxidizing conditions in long-lived humans.
450
451 Four, we uncovered a reciprocal relationship between *PRKN* expression and glutathione's
452 redox state *in vivo,* and generated evidence that parkin plays a direct role in GSSG
453 recycling. The thiol network, to which we propose parkin contributes, is critical in the
454 maintenance of overall redox balance, and thus, to cellular and organ health[41,42]. Here, we
455 expand on the observation made by Itier et al. by comparing a variety of cellular and
456 mouse models to human brain (**Fig. 3**). In parkin's absence: i) GSH is elevated to
457 increase the total number of free thiols; ii) GSSG levels are diminished; iii) the ratio of
458 GSH:GSSG is increased; and iv) total glutathione levels (GSH + GSSG) are unchanged,
459 except in bigenic mice (**Fig. 3c-f, h; Extended Data Fig. 4a-c, e**). We postulate that
460 parkin's presence reduced cellular needs for higher levels of free GSH. We first explored
461 *de novo* synthesis of GSH but found no increase in *GCLM* or *GCLC* mRNA levels. As
462 for the rise in total glutathione in bigenic mice, we reasoned that higher GSH levels may
463 still have resulted from *de novo* synthesis but via more effective translation of existing

464 *GCLM* mRNA[28,31], or elevated enzymatic activity, rather than by gene transcription. By
465 comparing results from the HPLC *vs.* GR-based quantification methods in murine brain,
466 we observed an increase in GSH levels and reciprocal decrease in GSSG levels in *prkn*$^{-/-}$
467 mice when using the latter method, which was therefore attributable to an increase in GR
468 enzyme-related activity (**Fig. 4a, f**)[30,31]. Because we had observed dynamic changes in
469 GSSG levels in cell models following increased parkin expression and oxidative stress
470 (**Fig. 3c-e**), we next explored whether parkin contributed to increased GSH levels by
471 direct thiol-mediated recycling of GSSG. There, we found that parkin directly bound to
472 GSSG in a concentration-dependent manner, which resulted in half of GSSG recycled to
473 GSH and the other half attached to parkin via S-glutathionylation (**Fig. 4b-e**).
474
475 The finding of parkin S-glutathionylation (**Fig. 4b, c**), and its reversal by glutaredoxin-1
476 and -2, further highlights the relevance of parkin's integration into redox chemistry. The
477 oxidation of proteins via S-glutathionylation represents a major contribution to redox
478 signaling and generally serves as a protective mechanism.[43,44] We noted with interest that
479 primate-specific cysteine 95 is targeted for oxidation by both S-glutathionylation (**Fig.**
480 **4e**) and dopamine radical adduct formation[10]. We question whether this specific residue,
481 which is located in the linker region of human parkin, could have an effect on parkin
482 activation akin to S65 phosphorylation during mitophagy. We anticipate that the many
483 posttranslational modifications of parkin, which we have identified here by LC-MS/MS,
484 will inform structurally oriented and cell biological research in the future. Such
485 investigations, which may focus on the linker region[33] and downstream mitochondrial
486 health[45] , should be explored in the context of parkin redox chemistry. Due to the
487 transient nature of S-glutathionylation (as well as of S-nitrosylation[39]) as a
488 posttranslational modification and due to the analytical methods used here (**Extended**
489 **Data Table 1**) and in our analyses of human brain[10], namely under reducing (and
490 alkylating) conditions, we have not yet validated parkin S-glutathionylation *in vivo*. We
491 hope to continue these investigations in the near future.
492
493 Future studies will also explore which region and which cell type in the nervous system[27]
494 contribute most significantly to the parkin-dependent glutathione redox changes we have

observed *in vivo*. The lack of significantly elevated GSH levels in *prkn*$^{-/-}$ mouse brain by HPLC suggests that this species can compensate for increased cytosolic ROS via other redox state-regulating mechanisms, such as via glutathione peroxidase (GPx) activity (**Fig. 4f**). High tolerance to ROS may help explain the lack of dopamine cell loss in *prkn*-null mice[18,26,46]. In aged mouse brain, one or more additional stressor could be required, such as demonstrated in the *prkn*$^{-/-}$//*Sod2*$^{+/-}$ mice. A human-specific redox aspect is that nigral neurons experience high levels of ROS production, dysregulated iron homeostasis, and more radical formation from oxidative dopamine metabolism[10,47,48]. Differences in human *vs.* murine parkin oxidative metabolism will thus be further explored.

The strengths of our investigations are three-fold: 1) results in cellular and murine models restaged findings in human tissues[10,19] (**Figs. 2h, i; 3f, g**); 2) our research integrated *in vitro, ex vivo, in situ* and *in vivo* paradigms as well as exogenous and endogenous ROS sources; and 3) the redox hypothesis of parkin function readily explains its many reported roles in distinct cellular paradigms, *e.g.,* cancer biology, mitochondrial health, immunity, etc.[49], because these pathways are (co-)regulated by redox state changes (**Fig. 4f**).

We have also identified shortcomings. First, in future work we will conduct a more extensive assessment of the diversity and quantity of oxidative modifications in brain parkin by LC-MS/MS, for example in our MPTP-exposed *vs.* untreated mouse model, in order to map additional *bona fide* oxidation sites that occur *in vivo*. As mentioned, we have yet to validate S-glutathionylation of parkin *in vivo*, which will require optimization of mass spectrometry techniques. Furthermore, we wish to study a greater number of *PRKN*-genotyped, age-matched, human brain tissue specimens to quantify protein carbonylation and nitrotyrosination, as well as to explore human brain-specific changes in redox state-related transcriptomes from different areas of the brain. Recently, we have begun to characterize glutathione-regulating enzyme levels *in vivo, e.g.,* glutathione-reductase, to validate our model that its activity is markedly increased in ARPD (**Fig. 4f**).

Our discovery that parkin's seemingly diverse activities are anchored in traditional redox chemistry (**Fig. 4f**) provides at once a biochemical and unifying explanation for its role in

neuroprotection. It may also help answer the two decades-old question: "What function of parkin is essential in conferring the selective protection of dopamine neurons in the adult human brainstem?"[10,50] Further exploration of parkin's redox effects should create new opportunities to develop urgently needed therapies for patients with young-onset, currently incurable parkinsonism.

570 **REFERENCES**

571 1 Mori, H. *et al.* Pathologic and biochemical studies of juvenile parkinsonism
572 linked to chromosome 6q. *Neurology* **51**, 890-892, doi:10.1212/wnl.51.3.890
573 (1998).
574 2 Zecca, L. *et al.* The role of iron and copper molecules in the neuronal
575 vulnerability of locus coeruleus and substantia nigra during aging. *Proc Natl Acad*
576 *Sci U S A* **101**, 9843-9848, doi:10.1073/pnas.0403495101 (2004).
577 3 Pacelli, C. *et al.* Elevated Mitochondrial Bioenergetics and Axonal Arborization
578 Size Are Key Contributors to the Vulnerability of Dopamine Neurons. *Curr Biol*
579 **25**, 2349-2360, doi:10.1016/j.cub.2015.07.050 (2015).
580 4 Giguere, N., Burke Nanni, S. & Trudeau, L. E. On Cell Loss and Selective
581 Vulnerability of Neuronal Populations in Parkinson's Disease. *Front Neurol* **9**,
582 455, doi:10.3389/fneur.2018.00455 (2018).
583 5 Burbulla, L. F. *et al.* Dopamine oxidation mediates mitochondrial and lysosomal
584 dysfunction in Parkinson's disease. *Science* **357**, 1255-1261,
585 doi:10.1126/science.aam9080 (2017).
586 6 Shimura, H. *et al.* Familial Parkinson disease gene product, parkin, is a ubiquitin-
587 protein ligase. *Nat Genet* **25**, 302-305, doi:10.1038/77060 (2000).
588 7 Matsuda, N. *et al.* PINK1 stabilized by mitochondrial depolarization recruits
589 Parkin to damaged mitochondria and activates latent Parkin for mitophagy. *J Cell*
590 *Biol* **189**, 211-221, doi:10.1083/jcb.200910140 (2010).
591 8 Narendra, D., Tanaka, A., Suen, D. F. & Youle, R. J. Parkin is recruited
592 selectively to impaired mitochondria and promotes their autophagy. *J Cell Biol*
593 **183**, 795-803, doi:10.1083/jcb.200809125 (2008).
594 9 LaVoie, M. J., Ostaszewski, B. L., Weihofen, A., Schlossmacher, M. G. &
595 Selkoe, D. J. Dopamine covalently modifies and functionally inactivates parkin.
596 *Nat Med* **11**, 1214-1221, doi:10.1038/nm1314 (2005).
597 10 Tokarew, J. M. *et al.* Oxidative Modifications of Parkin Underlie its Selective
598 Neuroprotection in Adult Human Brain. *bioRxiv*, 2020.2002.2019.953034,
599 doi:10.1101/2020.02.19.953034 (2020).
600 11 Schapira, A. H. & Gegg, M. Mitochondrial contribution to Parkinson's disease
601 pathogenesis. *Parkinsons Dis* **2011**, 159160, doi:10.4061/2011/159160 (2011).
602 12 Martinez, T. N. & Greenamyre, J. T. Toxin models of mitochondrial dysfunction
603 in Parkinson's disease. *Antioxid Redox Signal* **16**, 920-934,
604 doi:10.1089/ars.2011.4033 (2012).
605 13 Townsend, D. M., Tew, K. D. & Tapiero, H. The importance of glutathione in
606 human disease. *Biomed Pharmacother* **57**, 145-155, doi:10.1016/s0753-
607 3322(03)00043-x (2003).
608 14 Palacino, J. J. *et al.* Mitochondrial dysfunction and oxidative damage in parkin-
609 deficient mice. *J Biol Chem* **279**, 18614-18622, doi:10.1074/jbc.M401135200
610 (2004).
611 15 Periquet, M., Corti, O., Jacquier, S. & Brice, A. Proteomic analysis of parkin
612 knockout mice: alterations in energy metabolism, protein handling and synaptic
613 function. *J Neurochem* **95**, 1259-1276, doi:10.1111/j.1471-4159.2005.03442.x
614 (2005).

615 16 LaVoie, M. J., Cortese, G. P., Ostaszewski, B. L. & Schlossmacher, M. G. The
616 effects of oxidative stress on parkin and other E3 ligases. *J Neurochem* **103**, 2354-
617 2368, doi:10.1111/j.1471-4159.2007.04911.x (2007).
618 17 Andres-Mateos, E. *et al.* DJ-1 gene deletion reveals that DJ-1 is an atypical
619 peroxiredoxin-like peroxidase. *Proc Natl Acad Sci U S A* **104**, 14807-14812,
620 doi:10.1073/pnas.0703219104 (2007).
621 18 Goldberg, M. S. *et al.* Parkin-deficient mice exhibit nigrostriatal deficits but not
622 loss of dopaminergic neurons. *J Biol Chem* **278**, 43628-43635,
623 doi:10.1074/jbc.M308947200 (2003).
624 19 Pawlyk, A. C. *et al.* Novel monoclonal antibodies demonstrate biochemical
625 variation of brain parkin with age. *J Biol Chem* **278**, 48120-48128,
626 doi:10.1074/jbc.M306889200 (2003).
627 20 Ali, S. F., David, S. N., Newport, G. D., Cadet, J. L. & Slikker, W., Jr. MPTP-
628 induced oxidative stress and neurotoxicity are age-dependent: evidence from
629 measures of reactive oxygen species and striatal dopamine levels. *Synapse* **18**, 27-
630 34, doi:10.1002/syn.890180105 (1994).
631 21 Hinerfeld, D. *et al.* Endogenous mitochondrial oxidative stress:
632 neurodegeneration, proteomic analysis, specific respiratory chain defects, and
633 efficacious antioxidant therapy in superoxide dismutase 2 null mice. *J Neurochem*
634 **88**, 657-667, doi:10.1046/j.1471-4159.2003.02195.x (2004).
635 22 Spratt, D. E. *et al.* A molecular explanation for the recessive nature of parkin-
636 linked Parkinson's disease. *Nat Commun* **4**, 1983, doi:10.1038/ncomms2983
637 (2013).
638 23 Han, D., Antunes, F., Canali, R., Rettori, D. & Cadenas, E. Voltage-dependent
639 anion channels control the release of the superoxide anion from mitochondria to
640 cytosol. *J Biol Chem* **278**, 5557-5563, doi:10.1074/jbc.M210269200 (2003).
641 24 Shimura, H. *et al.* Ubiquitination of a new form of alpha-synuclein by parkin from
642 human brain: implications for Parkinson's disease. *Science* **293**, 263-269,
643 doi:10.1126/science.1060627 (2001).
644 25 Wiese, A. G., Pacifici, R. E. & Davies, K. J. Transient adaptation of oxidative
645 stress in mammalian cells. *Arch Biochem Biophys* **318**, 231-240,
646 doi:10.1006/abbi.1995.1225 (1995).
647 26 Itier, J. M. *et al.* Parkin gene inactivation alters behaviour and dopamine
648 neurotransmission in the mouse. *Hum Mol Genet* **12**, 2277-2291,
649 doi:10.1093/hmg/ddg239 (2003).
650 27 Solano, R. M. *et al.* Glial dysfunction in parkin null mice: effects of aging. *J*
651 *Neurosci* **28**, 598-611, doi:10.1523/JNEUROSCI.4609-07.2008 (2008).
652 28 Sikalidis, A. K. *et al.* Upregulation of capacity for glutathione synthesis in
653 response to amino acid deprivation: regulation of glutamate-cysteine ligase
654 subunits. *Amino Acids* **46**, 1285-1296, doi:10.1007/s00726-014-1687-1 (2014).
655 29 Tietze, F. Enzymic method for quantitative determination of nanogram amounts
656 of total and oxidized glutathione: applications to mammalian blood and other
657 tissues. *Anal Biochem* **27**, 502-522, doi:10.1016/0003-2697(69)90064-5 (1969).
658 30 Frasier, C. R. *et al.* Redox-dependent increases in glutathione reductase and
659 exercise preconditioning: role of NADPH oxidase and mitochondria. *Cardiovasc*
660 *Res* **98**, 47-55, doi:10.1093/cvr/cvt009 (2013).

661 31 Espinosa-Diez, C. *et al.* Antioxidant responses and cellular adjustments to
662 oxidative stress. *Redox Biol* **6**, 183-197, doi:10.1016/j.redox.2015.07.008 (2015).
663 32 Sengupta, R., Coppo, L., Mishra, P. & Holmgren, A. Glutathione-glutaredoxin is
664 an efficient electron donor system for mammalian p53R2-R1-dependent
665 ribonucleotide reductase. *J Biol Chem* **294**, 12708-12716,
666 doi:10.1074/jbc.RA119.008752 (2019).
667 33 Aguirre, J. D., Dunkerley, K. M., Mercier, P. & Shaw, G. S. Structure of
668 phosphorylated UBL domain and insights into PINK1-orchestrated parkin
669 activation. *Proc Natl Acad Sci U S A* **114**, 298-303, doi:10.1073/pnas.1613040114
670 (2017).
671 34 Berger, A. K. *et al.* Parkin selectively alters the intrinsic threshold for
672 mitochondrial cytochrome c release. *Hum Mol Genet* **18**, 4317-4328,
673 doi:10.1093/hmg/ddp384 (2009).
674 35 Feany, M. B. & Pallanck, L. J. Parkin: a multipurpose neuroprotective agent?
675 *Neuron* **38**, 13-16 (2003).
676 36 Chung, K. K. *et al.* S-nitrosylation of parkin regulates ubiquitination and
677 compromises parkin's protective function. *Science* **304**, 1328-1331,
678 doi:10.1126/science.1093891 (2004).
679 37 Meng, F. *et al.* Oxidation of the cysteine-rich regions of parkin perturbs its E3
680 ligase activity and contributes to protein aggregation. *Mol Neurodegener* **6**, 34,
681 doi:10.1186/1750-1326-6-34 (2011).
682 38 Komander, D. The emerging complexity of protein ubiquitination. *Biochem Soc*
683 *Trans* **37**, 937-953, doi:10.1042/BST0370937 (2009).
684 39 Yao, D. *et al.* Nitrosative stress linked to sporadic Parkinson's disease: S-
685 nitrosylation of parkin regulates its E3 ubiquitin ligase activity. *Proc Natl Acad*
686 *Sci U S A* **101**, 10810-10814, doi:10.1073/pnas.0404161101 (2004).
687 40 Vandiver, M. S. *et al.* Sulfhydration mediates neuroprotective actions of parkin.
688 *Nat Commun* **4**, 1626, doi:10.1038/ncomms2623 (2013).
689 41 Go, Y. M. & Jones, D. P. The redox proteome. *J Biol Chem* **288**, 26512-26520,
690 doi:10.1074/jbc.R113.464131 (2013).
691 42 Go, Y. M., Chandler, J. D. & Jones, D. P. The cysteine proteome. *Free Radic Biol*
692 *Med* **84**, 227-245, doi:10.1016/j.freeradbiomed.2015.03.022 (2015).
693 43 Xiong, Y., Uys, J. D., Tew, K. D. & Townsend, D. M. S-glutathionylation: from
694 molecular mechanisms to health outcomes. *Antioxid Redox Signal* **15**, 233-270,
695 doi:10.1089/ars.2010.3540 (2011).
696 44 Sabens Liedhegner, E. A., Gao, X. H. & Mieyal, J. J. Mechanisms of altered
697 redox regulation in neurodegenerative diseases--focus on S--glutathionylation.
698 *Antioxid Redox Signal* **16**, 543-566, doi:10.1089/ars.2011.4119 (2012).
699 45 Koyano, F. *et al.* Ubiquitin is phosphorylated by PINK1 to activate parkin. *Nature*
700 **510**, 162-166, doi:10.1038/nature13392 (2014).
701 46 Kitada, T. *et al.* Impaired dopamine release and synaptic plasticity in the striatum
702 of parkin-/- mice. *J Neurochem* **110**, 613-621, doi:10.1111/j.1471-
703 4159.2009.06152.x (2009).
704 47 Zucca, F. A. *et al.* Neuromelanin organelles are specialized autolysosomes that
705 accumulate undegraded proteins and lipids in aging human brain and are likely

involved in Parkinson's disease. *NPJ Parkinsons Dis* **4**, 17, doi:10.1038/s41531-018-0050-8 (2018).

48 Zucca, F. A. *et al.* Interactions of iron, dopamine and neuromelanin pathways in brain aging and Parkinson's disease. *Prog Neurobiol* **155**, 96-119, doi:10.1016/j.pneurobio.2015.09.012 (2017).

49 Xu, L., Lin, D. C., Yin, D. & Koeffler, H. P. An emerging role of PARK2 in cancer. *J Mol Med (Berl)* **92**, 31-42, doi:10.1007/s00109-013-1107-0 (2014).

50 Kitada, T., Tomlinson, J. J., Ao, H. S., Grimes, D. A. & Schlossmacher, M. G. Considerations regarding the etiology and future treatment of autosomal recessive versus idiopathic Parkinson disease. *Curr Treat Options Neurol* **14**, 230-240, doi:10.1007/s11940-012-0175-8 (2012).

752 **MATERIALS AND METHODS**
753

754 **Mouse tissues**

755 Brains and hearts were collected from wild-type C57Bl/6J from Jackson laboratories,
756 *prkn*-null from Dr. Brice's laboratory [26], *Sod2* +/- mice from Jackson laboratories; the
757 bigenic mouse ($prkn^{-/-}$//$Sod2^{+/-}$) was created by crossing *prkn*-null mice with *Sod2*
758 haploinsufficient mice, and interbreeding heterozygous offspring. The bigenic mouse will
759 be further characterized elsewhere (El Kodsi et al., in preparation). Mouse brains
760 collected were homogenized on ice in a Dounce glass homogenizer by 20 passes in Tris
761 salt buffer with or without the addition of 1% H_2O_2, transferred to ultracentrifuge tubes
762 and spun at 55,000 and 4°C for 30 mins to extract the soluble fraction. The resulting
763 pellets were further homogenized in the tris salt buffer with the addition of 2-10% SDS,
764 transferred to ultracentrifuge tubes and spun at 55,000 rpm and 10°C for 30 minutes to
765 extract the insoluble fraction.

766

767 **Cell culture, transfection and oxidation**

768 Human embryonic kidney (HEK293) were grown in Dulbecco's Modified Eagle Medium
769 (DMEM) supplemented with 1 % penicillin/streptomycin and 10 % heat-inactivated fetal
770 bovine serum (FBS) at 37°C with 5 % CO_2. Four to 15 µg of cDNA coding for N-
771 terminally flag-tagged parkin or empty Flag control vector (pcDNA3.1+) using a 1:1 ratio
772 of cDNA:Lipofectamine 2000, was used for ectopic overexpression. The cDNA and
773 Lipofectamine 2000 were incubated for 20 min at room temperature before being applied
774 directly to the cells for 1 hour at 37°C with 5 % CO_2 followed by direct addition of fresh
775 growth medium. Cells were incubated another 24 hours before treatment, harvesting and
776 analysis. Control Chinese hamster ovary cells, stably expressing the myc-vector (CHO),
777 or expressing myc-parkin (CHO-parkin) were also used.

778 All chemicals (H_2O_2, CCCP, NEM, IAA, DTT, AT, BSO and NAC) were added directly
779 to cells at ~75% confluence in growth or OPTI-MEM media. Cells were manually
780 scrapped, spun at a 1000 rpm for 5 minutes, the pellets washed with PBS and then

781 homogenized in a Tris salt buffer, transferred to ultracentrifuge tubes and spun at 55,000
782 rpm and 4°C for 30 minutes to extract the soluble fraction. The resulting pellets were
783 further homogenized in the Tris salt buffer with the addition of 2-10% SDS, transferred
784 to ultracentrifuge tubes and spun at 55,000 rpm and 10°C for 30 minutes to extract the
785 insoluble fraction. SH-SY5Y cells were generally seeded at a density of 0.5-1 x 106
786 cells/mL. Once cells reached 70-80 % confluency they were transfected with cDNA
787 coding for C-terminally Flag-tagged Parkin or empty Flag control vector (pcDNA3) by
788 electroporation using the nucleofector method described by Hu and Li, 2015. A total of 2
789 million cells were resuspended in 100 µL of OPTI-MEM containing cDNA (2 µg) and 1
790 % polyoxamer 188. The cells were electroporated using the X Unit and pulse code "CA-
791 137" on a Lonza 4D-Nucleofector. Following electroporation, cells were seeded at a
792 concentration of 0.8-1 x 106 cells/mL [51].
793
794 **Western blot and densitometry**
795 Brain homogenates and cell lysates were run on 4-12 % Bis-Tris SDS-PAGE gels using
796 MES running buffer. Proteins were transferred to PVDF membranes using transfer
797 buffer, and immunoblotted for parkin, DJ-1, MnSOD, aconitase-2, creatine kinase,
798 VDAC, TOM20, nitrotyrosine, and flag-epitopes. Actin and Ponceau S staining were
799 used as loading controls. For densitometry quantification, the signal intensity of parkin
800 from each sample was measured as pixel using Image J Software, and controlled for
801 loading, against actin's band intensity. Proteins were also stained in gel using Coomassie
802 brilliant blue R-250 dye. The gel was first fixed in 10% acetic acid, 50% methanol,
803 followed by staining for 2-24 hours with Coomassie and finally destained in 7.5% acetic
804 acid, 5% methanol until crisp blue bands appeared.
805
806 **MPTP treatment**

807 Eight to 12 months old WT and *prkn*-null mice were injected intraperitoneally with
808 40mg/kg of saline or MPTP and sacrificed an hour later [20]. The brains were harvested for
809 ROS measurement, protein analysis by Western blot and immunoprecipitation of parkin
810 and mass spectrometry analysis. For mass spectrometry, the brains harvested were first

811 incubated in IAA prior to homogenization and fractionation as described above. Brain
812 homogenates were then incubated with anti-parkin conjugated to magnetic beads
813 (Dynabeads Coupling Kit; Invitrogen). A magnet was used to capture parkin bound to the
814 beads, and several washes were used to remove unbound proteins. Eluted fractions (IP
815 elute) along with controls (input, unbound, wash and recombinant parkin protein
816 standards) were run on SDS/PAGE and blotted with anti-parkin. A sister gel was stained
817 with Coomassie as described above and gel slices corresponding to band sizes 50-75 kDa
818 were excised and analyzed by LC-MS/MS, as described in detail by Tokarew et al., 2020.

819

820 **Recombinant, tag-less protein expression in pET-SUMO vector**

821 Wild-type and truncated (residues 321-465) human parkin were expressed as 6His-Smt3
822 fusion proteins in *Escherichia coli* BL21 (DE3) Codon-Plus RIL competent cells (C2527,
823 New England Biolabs) as previous described[22,33,52]. DJ-1 and SNCA coding sequences
824 were cloned from a pcDNA3.1 vector into the pET-SUMO vector using PCR and
825 restriction enzymes. All proteins were overexpressed in *E. coli* BL21 Codon-Plus
826 competent cells (C2527, New England Biolabs) and grown at 37 °C in 2 % Luria Broth
827 containing 30 mg/L kanamycin until OD600 reached 0.6, at which point the temperature
828 was reduced to 16°C. Parkin protein-expressing cultures were also supplemented with 0.5
829 mM $ZnCl_2$. Once OD600 reached 0.8, protein expression was induced with isopropyl β-
830 D-1-thiogalactopyranoside, except ulp1 protease, which was induced once OD600 had
831 reached 1.2. The concentration of IPTG used for each construct is as follows: 25 μM for
832 wild-type and point mutants of parkin, and 0.75 mM for truncated parkin, DJ-1, α-
833 synuclein, SAG, and ulp1 protease. Cultures were left to express protein for 16-20 h.
834 Cells were then harvested, centrifuged, lysed and collected on Ni-NTA agarose beads in
835 elution columns.

836

837

838 **Recombinant maltose-binding protein-tagged protein expression in pMAL-2T**
839 **vector**

840 Wild-type and truncated (residues 327-465) human parkin were expressed in the pMAL-
841 2T vector (a gift from Dr. Keiji Tanaka), as previously described[53]. Parkin produced in
842 this vector contained an N-terminal maltose-binding protein (MBP) and thrombin
843 cleavage site (LVPRGS). All proteins were overexpressed in *E. coli* BL21 Codon-Plus
844 competent cells (C2527, New England Biolabs) and grown at 37 °C in 2 % Luria Broth
845 containing 0.2 % glucose and 100 mg/L ampicillin until OD600 reached 0.3-0.37, at
846 which point protein expression was induced with addition of 0.4 mM isopropyl β-D-1-
847 thiogalactopyranoside. Cultures were left to express protein at 37 °C until OD600
848 reached 0.9-1.0. Harvested protein isolates were purified using amylose resin in buffers
849 containing 100 μM zinc sulfate and 10 mM maltose.

850

851 **ROS (H_2O_2) measurements of recombinant proteins, tissue and cell lysates**

852 Amplex® Red hydrogen peroxide/peroxidase assay kit (Invitrogen A22188) was used to
853 monitor endogenous levels of H_2O_2 in tissues and cells, and residual levels of H_2O_2 after
854 incubation with recombinant parkin (WT, or pre-incubated with increasing
855 concentrations of H_2O_2, NEM, or EDTA), DJ-1, SNCA, BSA, RNF43 (from BioLegend),
856 HOIP (from Boston Biochem), GSH, catalase, NEM and EDTA for 30 minutes. Pre-
857 weighed cortex pieces from human brains (or pelleted cells) were homogenized on ice in
858 the 1x reaction buffer provided, using a Dounce homogenizer (3 times volume to weight
859 ratio). Homogenates were diluted in the same 1x reaction buffer (10x and 5x). A serial
860 dilution of the H_2O_2 standard provided was prepared (20, 10, 2 and 0 μM). 50 μL of
861 standards and samples were plated in a 96 well black plate with clear flat bottom. The
862 reaction was started by the addition of 50μL working solution which consist of 1x
863 reaction buffer, Amplex® red and horseradish peroxidase. The plate was incubated at
864 room temperature for 30 minutes protected from light. A microplate reader was used to
865 measure either fluorescence with excitation at 560 nm and emission at 590 nm, or
866 absorbance at 560 nm. The obtained H_2O_2 levels (μM) were normalized to the tissue

867 weight (g) or protein concentration (μg/μL). The same aasay was also used to measure
868 parkin and glutathione's peroxidase activity compared to horseradish peroxidase (HRP).

869

870 **ROS (H_2O_2) measurements of intact cells**

871 HEK293 cells were transfected with flag-parkin or control vector (pcDNA) as described
872 above. After 24 h the cells were lifted using trypsin and re-seeded in a 12-well dish at a
873 density of 0.3 x 106 cells/mL. After 48 h the cells were treated with 0 mM or 2 mM H_2O_2
874 in OPTI-MEM medium at 37°C and 5 % CO_2. After 1 h the cells were washed with
875 OPTI-MEM and incubated with 20 μM of dichlorofluorescin diacetate (DCFH-DA,
876 D6883, Sigma) for 30 min at 37°C and 5 % CO_2. Cells were collected using a cell lifter
877 and treated with ethidium-1 dead stain (E1169, Invitrogen) for 15 min at room
878 temperature. Samples were analyzed using a BD Fortessa flow cytometer set to measure
879 the ROS-sensitive probe (DCFH-DA, ex. 488 nm and em. 527 nm) and viability stain
880 (ethidium-1, ex, 528 nm and em. 617 nm). The results were reported as the average mean
881 fluorescence intensity (MFI) of ROS in live cells. Each separate transfection was
882 considered one biological replicate.

883

884 **Cell cytotoxicity assay**

885 Vybrant ™ cytotoxicity assay kit (Molecular Probes V-23111) was used to monitor cell
886 death through the release of the cytosolic enzyme glucose 6-phosphate dehydrogenase
887 (G6yPD) from damaged cells into the surrounding medium. 50μl of media alone (no
888 cells), media from control and stressed CHO-parkin and control cells and cell lysates
889 were added to a 96-well microplate. 50 μl of reaction mixture, containing reaction buffer,
890 reaction mixture and resazurin, was added to all wells, and the mircroplate was incubated
891 at 37°C for 30 mins. A microplate reader was used to measure either fluorescence with
892 excitation at 560 nm and emission at 590 nm. A rise in fluoresence indicates a rise in
893 G6PD levels i.e. a rise in cell death.

894

895 **Mitochondria isolation**

896 Fresh tissue was cut with scissors into manageable pieces, rinsed in cold PBS, then
897 homogenized using either a Dounce homogenizer or Warning blender in the presence of
898 twice the tissue volume of buffer A (20mM Hepes pH 7.4, 220mM mannitol, 68mM
899 sucrose, 80mM KCl, 0,5mM EGTA, 2mM $Mg(Ac)_2$, 1mM DTT, 1X protease inhibitor
900 (Roche)). The sample was centrifuged at 4070g in a tabletop centrifuge for 20 minutes at
901 4^oC. The supernatant was collected and spun again as above. The resulting supernatant
902 was spun at 10 000g for 20 minutes at 4^oC and the pellet was then washed in the above
903 buffer and spun again at 10 000g for 20 minutes. The resulting mitochondrial pellet was
904 carefully resuspended in buffer B (20mM Hepes pH 7.4, 220mM mannitol, 68mM
905 sucrose, 80mM KCl, 0,5mM EGTA, 2mM $Mg(Ac)_2$, 10% glycerol), aliquoted, and snap
906 frozen.

907

908 **Aconitase assay**

909 The Aconitase Enzyme Activity Microplate Assay Kit (MitoSciences) was used to
910 measure aconitase activity in mitochondria isolated from wild type and parkin knock-out
911 mouse brains as per manufacturer's instructions. Two brains each from 12 months old
912 mice were pooled to provide the mitochondria samples and normalized for total protein
913 concentration. These were treated with 0 or 4 μM H_2O_2 just prior to assay. The catalytic
914 conversion of isocitrate to cis-aconitate by aconitase was measured by quantifying the
915 amount of cis-aconitate in the reaction by reading the samples at 240nm. Rates in
916 μM/min were determined from 3 independent experiments performed in triplicate.

917

918 **Creatine kinase assay**

919 The EnzyChrom Creatine Kinase Assay Kit (BioAssay Systems) was applied to measure
920 creatine kinase activity in mitochondria purified from wild type and parkin knock-out
921 mouse brains following the manufacturer's instructions. Two brains were pooled each
922 from 12 months old mice to provide the mitochondrial samples and normalized for total
923 protein concentration. Mitochondria were incubated with 0 or 0.5mM H_2O_2 at room
924 temperature for 20 minutes prior to assay. The creatine kinase-dependent catalytic

925 conversion of creatine phosphate and ADP to creatine and ATP, was quantified indirectly
926 by measuring NADPH at 340nm. The ATP produced by the reaction phosphorylates
927 glucose to glucose-6-phosphate by hexokinase, which is then oxidized by NADP in the
928 presence of glucose-6-phosphate dehydrogenase, yielding NADPH. Rates in μM/min
929 were calculated for 3 independent experiments done in triplicate.
930

931 **GSH and GSSG quantification - HPLC**

932 Human and mouse brain pieces, and CHO cell pellets were homogenized in buffer
933 containing 125 mM sucrose, 5 mM TRIS, 1.5 mM EDTA, 0.5%TFA and 0.5%MPA in
934 mobile phase. Then samples were spun at 14000xg at 4 °C for 20 mins. Supernatants
935 were collected and analyzed using an Agilent HPLC system equipped with a Pursuit
936 C_{18} column (150 ×4.6 mm, 5 μm; Agilent Technologies) operating at a flow rate of
937 1 ml/min or. The mobile phase consisted of 0.09% trifluoroacetic acid diluted in ddH2O
938 and mixed with HPLC-grade methanol in a 90:10 ratio. Standard solutions were used to
939 estimate the retention times for GSH and GSSG. Using Agilent Chemstation software,
940 absolute amounts of GSH and GSSG were acquired by integrating the area under the
941 corresponding peaks, and values were calculated from standard curves

942

943 **GSH concentration determination by monochlorobimane assay**

944 Stock solutions of assay dye (monochlorobimane (MCB), 22 mM) and glutathione-S-
945 transferase (50 units/mL) were prepared in PBS and stored protected from light at -20°C.
946 The working solution was prepared using 12.8 μL of stock mcB and 80 μL of stock
947 glutathione-S-transferase in 4 mL PBS and stored on ice. Samples were prepared as
948 follows: cells were lifted mechanically using cell-lifters, washed twice and re-suspended
949 in ice-cold PBS, mixed by vortex and incubated on ice for 30 min. Following two freeze
950 thaw cycles using solid CO_2, the samples were sonicated 1 min on wet ice (S220 Ultra-
951 sonicator from Covaris) and spun at 3000 x g, 4°C, for 5 min. Total protein concentration
952 of supernatants was determined using Bradford assay. Samples and glutathione (GSH)
953 standards (0- 13 μM) were plated in 25 μL aliquots in a 96-well plate with clear bottom

954 and black sides. 25 µL of working solution was added to all experimental wells and
955 protected from light for 15 min at room temperature. Fluorescence (ex 380 nm, em 461
956 nm) was measured using a Synergy H1Multi-Mode Plate Reader (Bio Tek). The amount
957 of GSH detected in each sample was calculated using the regression curve obtained from
958 the glutathione standards.

959

960 **Tietze's enzymatic recycling determination of GSH and GSSG**

961 The enzymatic recycling method described by Rahman et al.[54] was used to determine
962 reduced glutathione (GSH) and oxidized glutathione (GSSG) levels in mouse brain
963 lysates. Hemi-brains of wild type (n=3) and parkin KO (n=3) mice, at 13 and 11 months
964 of age respectively, were collected, weighed and homogenized in 3X volume/weight of
965 KPEX (0.1 M potassium phosphate, 5 mM EDTA, 0.1 % Triton X-100, 0.6 %
966 sulfosalicylic acid, pH 7.5) using a glass Dounce homogenizer (50 passes). Samples were
967 spun at 8000 x g, 4°C, for 5 min and the supernatant protein concentration was
968 determined using Bradford assay. To determine the total glutathione (GSH + GSSG)
969 concentration, the following stock solutions were freshly prepared in KPE (0.1 M
970 potassium phosphate, 5 mM EDTA, pH 7.5): 5,5'-dithio-bis-[2-nitrobenzoic acid]
971 (DNTB) at 0.6 mg/mL, nicotinamide adenine dinucleotide phosphate (NADPH) at 0.6
972 mg/mL and glutathione reductase at 3 units/mL. GSH standards were prepared in KPE at
973 concentrations of 0-26 nM/mL. 20 µL of diluted sample or GSH standard was added per
974 well and 120 µL of a 1:1 mixture of the DNTB and glutathione reductase stocks solutions
975 was added to each assayed well. After 30 sec incubation, 60 µL of the NADPH was
976 added and absorbance was immediately measured at 412 nm in 30 sec intervals for a total
977 of 2 min. To determine the concentration of oxidized glutathione (GSSG), the samples
978 were first diluted (1 in 4) in KPE and treated with 0.2 % 2-vinylpyridine for 1 h at room
979 temperature. Excess vinyl-pyridine was quenched with 1 % triethanolamine and GSSG
980 was measured using the same method as total glutathione except GSH standards were
981 replaced with GSSG standards (0-26.24 nM/mL) that were treated with vinyl-pyridine
982 and triethanolamine. The absolute values of total glutathione (GSH + GSSG) and
983 oxidized glutathione (GSSG) per sample were calculated using the linear regression

984 obtained from the change in absorbance/min plotted against the GSH or GSSG standard
985 concentrations, respectively, and dividing by the total protein concentration. Absolute
986 values for GSH were determined using the following equation: GSH= [GSH + GSSG] –
987 2[GSSG] [54].

988

989 **Parkin-catalyzed redox state recycling**

990 Parkin protein buffer exchange to T200 protein buffer (50 mM Tris, 200 mM NaCl, pH
991 7.5) was first performed using repeat centrifugations (8 times 4000 x g at 4°C for 10 min)
992 in Amicon Ultra 10 kDa MWCO filters. Protein concentration was adjusted to 10 μM
993 using T200. Both reduced (GSH) and oxidized (GSSG) glutathione stocks were prepared
994 in phosphate buffered saline at concentrations of 1 mg/mL (3250 μM) and 2.01 mg/mL
995 (6560 μM) respectively. Glutathione standards of 0, 2.5, 5, 10 μM and 100 μM of both
996 GSH and GSSG were prepared and combined in the following ratios to a final volume of
997 90 μL at: 10 μM GSH: 0 μM GSSG, 9 μM GSH: 1 μM GSSG, 8 μM GSH: 2 μM GSSG,
998 6 μM GSH: 4 μM GSSG, 4 μM GSH: 6 μM GSSG, 2 μM GSH: 8 μM GSSG, 1 μM
999 GSH: 9 μM GSSG, and 0 μM GSH: 10 μM GSSG. R-parkin (1 μL of a 10 μM solution)
1000 was added to the prepared mixtures and allowed to incubate at room temperature for 15
1001 min. Samples were analyzed for GSH concentration using the monochlorobimane assay
1002 described above.

1003

1004 **Glutathionylation assay**

1005 Glutathionylation of tagged and untagged parkin proteins was performed, as described
1006 previously [55]. MBP-tagged parkin proteins were eluted from columns with excess
1007 maltose. Concentrated eluates were supplemented with 0.1% DMSO (10 μl DMSO in 10
1008 ml PBS), and excess DTT and maltose were removed by several cycles of centrifugation
1009 with 30 kDa cut-off filters. Proteins/peptides (14 μM) were incubated with 3 mM GSH
1010 for 1 h and then with 5 mM GSSG for 2 h at room temperature. Trypsin digestion was
1011 performed (Peptide: Trypsin = 20: 1) overnight at 4 °C. The Trypsin-digested fragments

1012 were run through MALDI analysis. To assay S-glutathionylation, the eosin-labeled GSSG
1013 (Di-E-GSSG) was used to glutathionylate proteins, as described previously [32]. Di-E-
1014 GSSG has quenched fluorescence in the disulphide form, which increases ~20-fold upon
1015 reduction of its disulphide bond and formation of E-GSH. Blackened 96-well-plates were
1016 used in a PerkinElmer Victor3 multilabel counter containing a final well volume of 200
1017 μl in 0.1 M potassium phosphate buffer (pH 7.5), 1 mM EDTA. The reaction was started
1018 by addition of 20 μM Di-E-GSSG to parkin proteins, followed by recording the
1019 fluorescence emission at 545 nm after excitation at 520 nm. Controls with no peptide
1020 added were used as fluorescent background. To confirm S-glutathionylation, reaction
1021 products were incubated with Di-E-GSSG. Aliquots of S-glutathionylated proteins were
1022 further treated with 10 mM DTT or with the complete GSH-Grx system. All samples
1023 were run on a non-reducing SDS-PAGE 4–12% acrylamide. The gel was exposed to UV
1024 transilluminator to visualize eosin-tagged glutathionylated protein. The same gels were
1025 later stained with Coomassie Blue staining. Di-Eosin-GSSG was purchased form IMCO,
1026 Sweden. Human Grx1, and Grx2 were prepared as described previously [32]. Rat
1027 recombinant TrxR was a kind gift from Prof. Elias Arner.
1028

1029 **Mass spectrometry analysis of glutathionylated parkin**

1030 The protein was treated with proteolytic digestion, using trypsin. The resulting peptides
1031 were separated using one dimension of liquid chromatography. The LC eluent was
1032 interfaced to a mass spectrometer using electrospray ionization and the peptides were
1033 analyzed by MS.

1034 LC−MS/MS analyses were performed using an Easy-nLC chromatography system
1035 directly coupled online to a Thermo Scientific Q Exactive hybrid quadrupole-Orbitrap
1036 mass spectrometer with a Thermo Scientific™ Nanospray Flex™ ion source. The sample
1037 was injected from a cooled autosampler onto a 10 cm long fused silica tip column
1038 (SilicaTips, New Objective, USA) packed in-house with 1.9 μm C18-AQ ReproSil-Pur
1039 (Dr. Maisch, Germany). The chromatographic separation was achieved using an
1040 acetonitrile (ACN)/ water solvent system containing 0,1% FA and a gradient of 60 min
1041 from 5 to 35% of ACN. The flow rate during the gradient was 300 nL/ min.

1042 MS/MS data were extracted and searched against in-house Mascot Server, (Revision
1043 2.5.0)**,** search engine that uses mass spectrometry data to identify and characterize
1044 proteins from sequence databases. The following parameters were used: trypsin digestion
1045 with a maximum of two missed cleavages; Carbamidomethyl (C), Oxidation (M),
1046 Deamidated (NQ) and Glutathione (G) as variable modifications; and a precursor mass
1047 tolerance of 10 ppm and a fragment mass tolerance of 0.02 Da. The identified protein was
1048 filtered using 1% false discovery rate (FDR) and at least two peptides per protein as
1049 limiting parameters.

1050

1051 **Protein carbonyl assay**

1052 Protein carbonyl colorimetric assay kit (Cayman chemical 10005020) was used to assay
1053 the carbonyl content in human and mouse brains or hearts. Pre-weighed tissues were
1054 rinsed in PBS and then homogenized in 1 mL cold PBS at pH 6.7 supplemented with 1
1055 mM EDTA, using a Dounce homogenizer on ice. Homogenates were centrifuged at
1056 10,000xg for 15 minutes at 4 °C. 200 µL of the supernatant was added to a tube with 800
1057 µL DNPH (sample tube) and 200 µL of the supernatant was added to a tube with 800 µL
1058 2.5 M HCL (control tube), both tubes were incubated in the dark for 1 hour with
1059 occasional vortex. 1 mL 20 % TCA followed by 1 mL 10% TCA solutions were added to
1060 centrifuged (10,000xg 10 minutes at 4 °C) pellet after discarding the supernatant. The
1061 resulting pellet was resuspended in1 mL of 1:1 ethanol:ethyl acetate mixture and
1062 centrifuged 3 times to extract protein pellets. The final pellets were suspended in 500 µL
1063 guanidine hydrochloride and centrifuged. A total of 220 µL per sample and control
1064 supernatants were added to two wells of a 96-well plate, and the absorbance was measure
1065 at 360 nm. The corrected absorbance (sample – control) was used in the following
1066 equation to obtain the protein carbonyl concentration: Protein Carbonyl (nmol/mL) =
1067 [(CA)/(0.011 μ M^{-1})](500 µL/200 µL). Total protein concentration from the sample
1068 tissues were measured to obtain the carbonyl content: protein carbonyl/total protein
1069 concentration.

1070

1071 **MnSOD activity assay**

1072 Superoxide dismutase assay kit (Cayman chemical 706002) was used to assay MnSOD
1073 activity in mouse brains. Pre-weighed perfused mouse brain pieces were homogenized in
1074 5 mL cold 20 mM HEPES buffer, pH 7.2, supplemented with EGTA, mannitol and
1075 sucrose, with a Dounce homogenizer on ice. The homogenates were centrifuged at
1076 1,500xg 5 minutes at 4 °C. The SOD standards were prepared by adding 200 µL of the
1077 radical detector and 10 µL of the provided standards, in duplicates in a 96-well plate. The
1078 same was repeated for the samples. The reaction was initiated by adding 20 µL of
1079 xanthine oxidase to all the wells. Background absorbance was assayed by adding 20 µL
1080 xanthine oxidase to sample buffer (optional). The plate was incubated on a shaker for 30
1081 minutes at room temperature. The absorbance was measure at 450 nm. The linearized
1082 SOD standard curve was plotted and used to calculate the MnSOD activity (U/mL) from
1083 the averaged sample absorbances.

1084

1085 **Total RNA isolation, cDNA synthesis and PCR amplification**

1086 Pre-weighed cortex pieces from mouse brains were homogenized in QIAzol (Qiagen
1087 79306), at 1ml volume per 100mg of tissue, and incubated at room temperature for 5
1088 minutes. 0.2mL of chloroform (per 1mL QIAzol) was added and the homogenates were
1089 shaken vigorously for 15 seconds, followed by a 2-3 minutes incubation at room
1090 temperature, the tubes were centrifuged at 12,000xg for 15 minutes at 4°C. The upper
1091 clear aqueous layer was transferred to a new tube and 1 volume of 70% ethanol was
1092 added, and mixed by vortexing. The solution was then added to an RNAeasy Mini spin
1093 column (Qiagen 74104) placed in a 2mL collection tube and centrifuged for 15 sec at
1094 8000xg at room temperature. The flow-through was discarded and 700 µL Buffer RW1
1095 was added to the spin column and spun for 15 sec at 8,000xg. The same step was
1096 repeated with 500 µL Buffer RPE, one spin for 15 sec and a second spin for 2 min. An
1097 optional spin in a new collection tube at full speed for 1 min to remove excess buffer was
1098 be added. The RNAeasy Mini spin column was placed in a new collection tube, 50 µL
1099 RNase-free water was added directly to the membrane and centrifuged for 1 minute at

1100 8000xg. A NanoDrop machine was used to measure the amount of total RNA obtained
1101 from the cortices. Turbo DNA-free™ (Life Technologies 1412059) was used to remove
1102 trace to moderate amounts of contaminating DNA. SuperScrpit™ IV First-Strand
1103 Synthesis System (Invitrogen 18091050) was used for cDNA synthesis reaction. iTaq™
1104 Universal SYBR® Green Supermix (BIO-RAD 172-5121) and select primer sets were
1105 used for PCR amplification of the newly synthesized cDNA templates, and controls, and
1106 analyzed by agarose gel electrophoresis and ethidium bromide staining. The following
1107 primers were used [56-58]:

1108 DJ-1, F: ATCTGAGTCGCCTATGGTGAAG; R: ACCTACTTCGTGAGCCAACAG

1109 GCLC, F: ATGTGGACACCCGATGCAGTATT; R: TGTCTTGCTTGTAGTCAGGATGGTTT

1110 GCLM, F: GCCACCAGATTTGACTGCCTTT; R: CAGGGATGCTTTCTTGAAGAGCTT

1111 Actin, F: CTTCCTCCCTGGAGAAGAGC; R: AAGGAAGGCTGGAAAAGAGC

1112

1113 **Statistical analyses**

1114 All statistical analyses were performed using GraphPad Prism version 8 (GraphPad
1115 Software, San Diego, CA, USA, www.graphpad.com). Differences between two groups
1116 were assessed using an unpaired t-test. Differences among 3 or more groups were
1117 assessed using a 1way or 2way ANOVA followed by Tukey's post hoc corrections to
1118 identify statistical significance. Subsequent post hoc tests are depicted graphically and
1119 show significance between treatments. For all statistical analysis a cut-off for
1120 significance was set at 0.05. Data is displayed with p values represented as *$p < 0.05$, **p
1121 < 0.01, ***$p < 0.001$, and ****$p < 0.0001$.

1122

1123

1124

1125

1126 **MATERIALS AND METHODS REFERENCES**

1127 51 Hu, J. & Li, S. Electroporation formulation for cell therapy. *Methods Mol Biol*
1128 **1121**, 55-60, doi:10.1007/978-1-4614-9632-8_4 (2014).
1129 52 Kumar, A. *et al.* Disruption of the autoinhibited state primes the E3 ligase parkin
1130 for activation and catalysis. *EMBO J* **34**, 2506-2521,
1131 doi:10.15252/embj.201592337 (2015).
1132 53 Matsuda, N. *et al.* Diverse effects of pathogenic mutations of Parkin that catalyze
1133 multiple monoubiquitylation in vitro. *J Biol Chem* **281**, 3204-3209,
1134 doi:10.1074/jbc.M510393200 (2006).
1135 54 Rahman, I., Kode, A. & Biswas, S. K. Assay for quantitative determination of
1136 glutathione and glutathione disulfide levels using enzymatic recycling method.
1137 *Nat Protoc* **1**, 3159-3165, doi:10.1038/nprot.2006.378 (2006).
1138 55 Casagrande, S. *et al.* Glutathionylation of human thioredoxin: a possible crosstalk
1139 between the glutathione and thioredoxin systems. *Proc Natl Acad Sci U S A* **99**,
1140 9745-9749, doi:10.1073/pnas.152168599 (2002).
1141 56 Diaz, D. *et al.* Tissue specific changes in the expression of glutamate-cysteine
1142 ligase mRNAs in mice exposed to methylmercury. *Toxicol Lett* **122**, 119-129,
1143 doi:10.1016/s0378-4274(01)00341-1 (2001).
1144 57 Shi, S. Y. *et al.* DJ-1 links muscle ROS production with metabolic
1145 reprogramming and systemic energy homeostasis in mice. *Nat Commun* **6**, 7415,
1146 doi:10.1038/ncomms8415 (2015).
1147 58 Abelev, B. I. *et al.* Longitudinal double-spin asymmetry and cross section for
1148 inclusive jet production in polarized proton collisions at square root of s = 200
1149 GeV. *Phys Rev Lett* **97**, 252001 (2006).

1150
1151
1152
1153
1154
1155
1156
1157
1158
1159
1160
1161

1162 **ACKNOWLEDGMENTS**

1163 We are grateful for the commitment of patients and their family members to participate in
1164 autopsy studies. We thank Drs. A. Brice and E. Fon for sharing *prkn*-null mice, Drs. N.
1165 Matsuda and K. Tanaka for MBP-parkin cDNA-encoding plasmids; Drs. R. Tam, S.
1166 Bennett and D. Pratt for helpful discussions, and members of the Schlossmacher lab for
1167 their critical comments and suggestions. **Funding:** This work was supported by the:
1168 Parkinson Research Consortium of Ottawa (D.N.E.K., J.M.T., J.J.T.); Queen Elizabeth II
1169 Graduate Scholarship Fund (J.M.T.); Government of Canada [CIHR MD/PhD Program
1170 (J.M.T., A.C.N.); NINDS/NIH (to M.J.L.); CIHR Research Grants (G.S.S., M.E.H.);
1171 CIHR Canada Research Chair Program (M.G.S.; G.S.S.)]; Michael J. Fox Foundation for
1172 Parkinson's Research (J.J.T., L.Z., M.G.S.); Uttra and Sam Bhargava Family (M.G.S.);
1173 and The Ottawa Hospital (M.G.S.). **Author contributions:** *Study design:* D.N.E.K.,
1174 J.M.T., J.J.T., M.G.S.; *Writing and figure preparation:* D.N.E.K., J.M.T., N.A.L., J.J.T.
1175 and M.G.S. prepared the initial draft of the manuscript and figures. All authors reviewed
1176 and / or edited the manuscript and approved of the submitted version. *Experiments*:
1177 D.N.E.K., J.M.T., N.A.L., R.S., A.C.N., H.B., C.P., B.S., D.S.I., L.Z., and L.P.
1178 performed experiments; R.S., C.P, J.A.C, M.T, N.H., R.R.R. and L.P provided data,
1179 tissue specimens and critical comments. *Analysis:* D.N.E.K. J.M.T, J.L., J.J.T., and
1180 M.G.S. performed data analyses. *Study supervision*: J.J.T. and M.G.S. *Overall*
1181 *responsibility:* M.G.S. This work is dedicated to the memories of Mr. Bruce Hayter
1182 (1962-2019), a tireless advocate for persons with young-onset parkinsonism, and our
1183 colleague, Dr. Arne Holmgren (1940-2020), a pioneer in redox biology.

1184

1185 **Additional Information:**

1186 **Data and materials availability**: Original data associated with this study are available in
1187 the main text and extended data figures and tables; additional data will be made available
1188 upon request.

1189

1190 **Supplementary Information** is available for this manuscript.

1191

1192 **Correspondence and requests for materials** should be addressed to J.J.T or M.G.S.

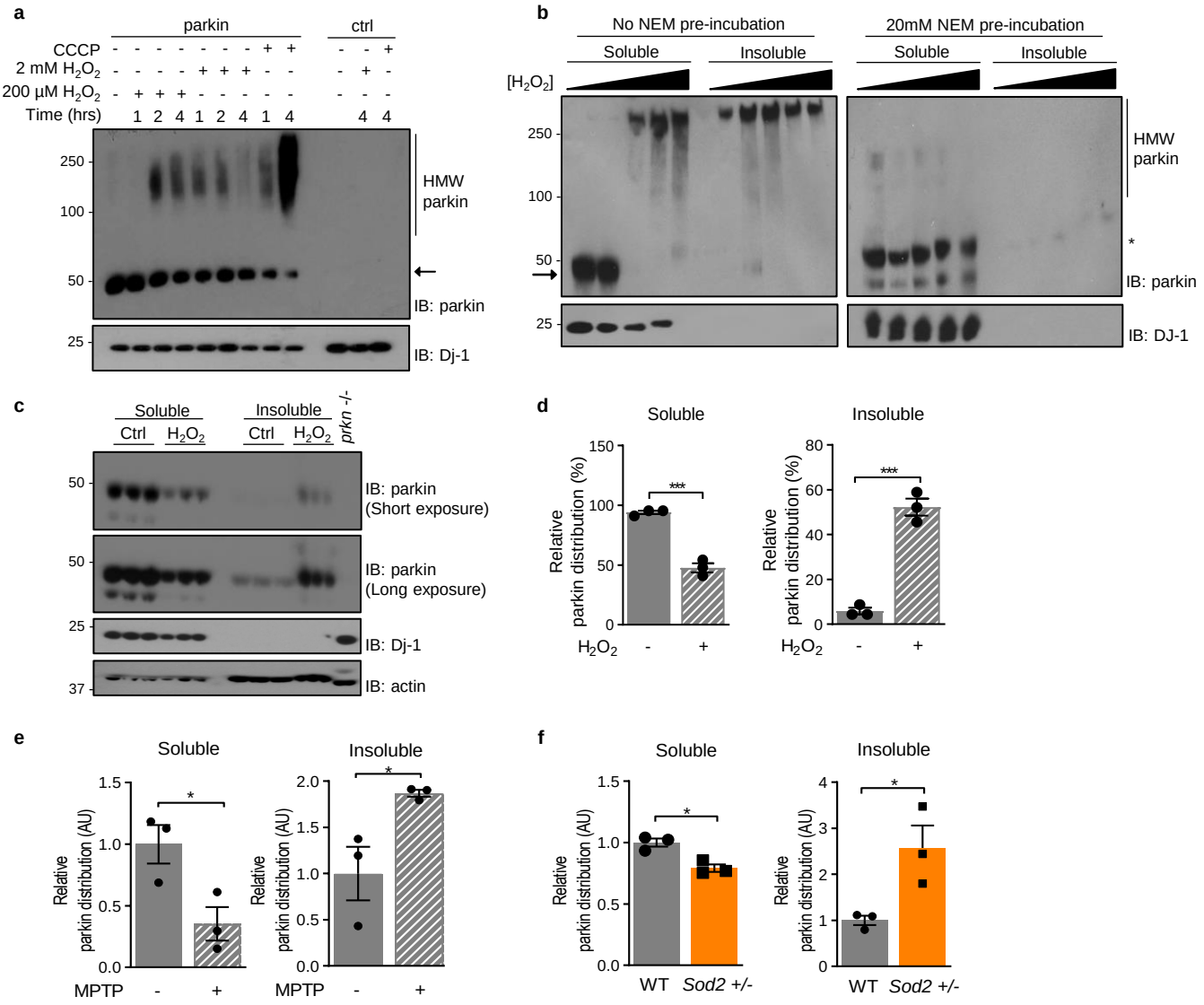

Figure 1: Mitochondrial and cytosolic stressors lead to oxidation of cellular parkin promoting its insolubility. Representative Western blots of parkin and Dj-1 distribution in, **a**, CHO-parkin and control cells under oxidizing conditions (200µM and 2mM H_2O_2; and 10µM CCCP), **b**, soluble and insoluble fractions from HEK293-parkin and control cells incubated with increasing concentrations of H_2O_2 (2µM to 2M) with or without 20mM n-ethylmaleimide (NEM) pre-incubation, and **c**, soluble and insoluble fraction from 2-4 mths-old wild-type C57Bl/6 mouse brains incubated with saline or 1% H_2O_2. (←) Monomeric parkin (*) Alkylated-parkin. Quantification of parkin's signal distribution in brain homogenates from, **d**, 2-4 mths-old wild-type C57Bl/6 mouse brains incubated with saline or 1% H_2O_2, **e**, 2-4 mths-old wild-type C57Bl/6 mice treated with a 40mg/kg intraperitoneal injection of MPTP toxin or saline. **f**, 6-8 mths-old C57Bl/6 wild-type (WT) and *Sod2*$^{+/-}$ mouse brains (soluble and insoluble fractions are shown). A Student t-test was used for statistical analysis (* = < 0.05, *** = <0.001).

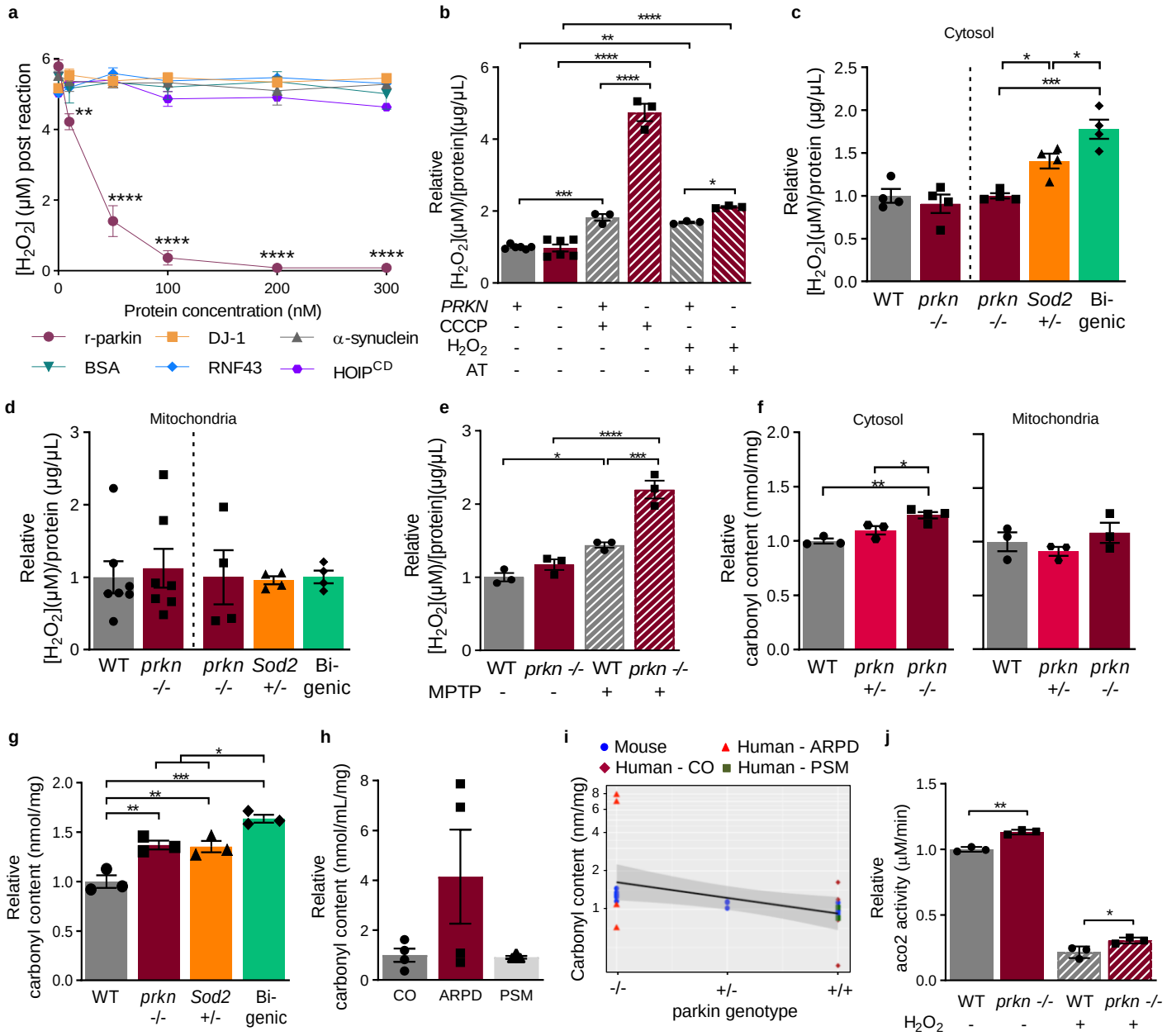

Figure 2: Parkin cysteines reduce hydrogen peroxide to lower oxidative stress.
a, Parkin's reducing capacity compared to DJ-1, α-synuclein, bovine serum albumin (BSA), and two RING-carrying ubiquitin ligases (RNF43 and HOIP^{cd}, (^{cd} - catalytic domain)). **b**, Endogenous levels of H_2O_2 in HEK293-parkin and control cells under control *vs.* oxidizing conditions [10μM CCCP for 1hr; 0.5M AT (to inhibit catalase) + 2mM H_2O_2 for 30mins]. Endogenous levels of H_2O_2 in **c**, cytosol-enriched and in **d**, mitochondria-rich brain homogenates of 6-8 mths-old WT and *prkn*$^{-/-}$ and, 2-4 mths-old *prkn*$^{-/-}$, *Sod2*$^{+/-}$ and bi-genic (*prkn*$^{-/-}$//*Sod2*$^{+/-}$) C57Bl/6 mice, and in **e**, 6-8 mths-old WT or *prkn*$^{-/-}$ mouse brains treated *in vivo* with either saline or MPTP toxin. Protein carbonyl content in **f**, cytosol-enriched and mitochondria-rich brain homogenates from 8 mths-old WT, *prkn*$^{+/-}$, and *prkn*$^{-/-}$ mouse brains, **g**, brain lysates of 6 mths old WT, *prkn*$^{-/-}$, *Sod2*$^{+/-}$ and bigenic mice, and **h**, aged-matched cortex specimens from controls, *PRKN*-deficient ARPD patients and subjects with other forms of parkinsonism (PSM). **i**, Carbonyl content (nmol/mL/mg) in mammalian brains of different *PRKN* genotypes. Linear regression line (blue) with standard error (gray shade) signals the overall trend. **j,** Aconitase-2 enzyme activity in mitochondria isolated from 12 mths-old WT and *prkn*$^{-/-}$ mouse brains. 1-way or 2-way ANOVA was used for statistical analysis (* = < 0.05; ** = < 0.01; *** = < 0.001; and ****= <0.0001).

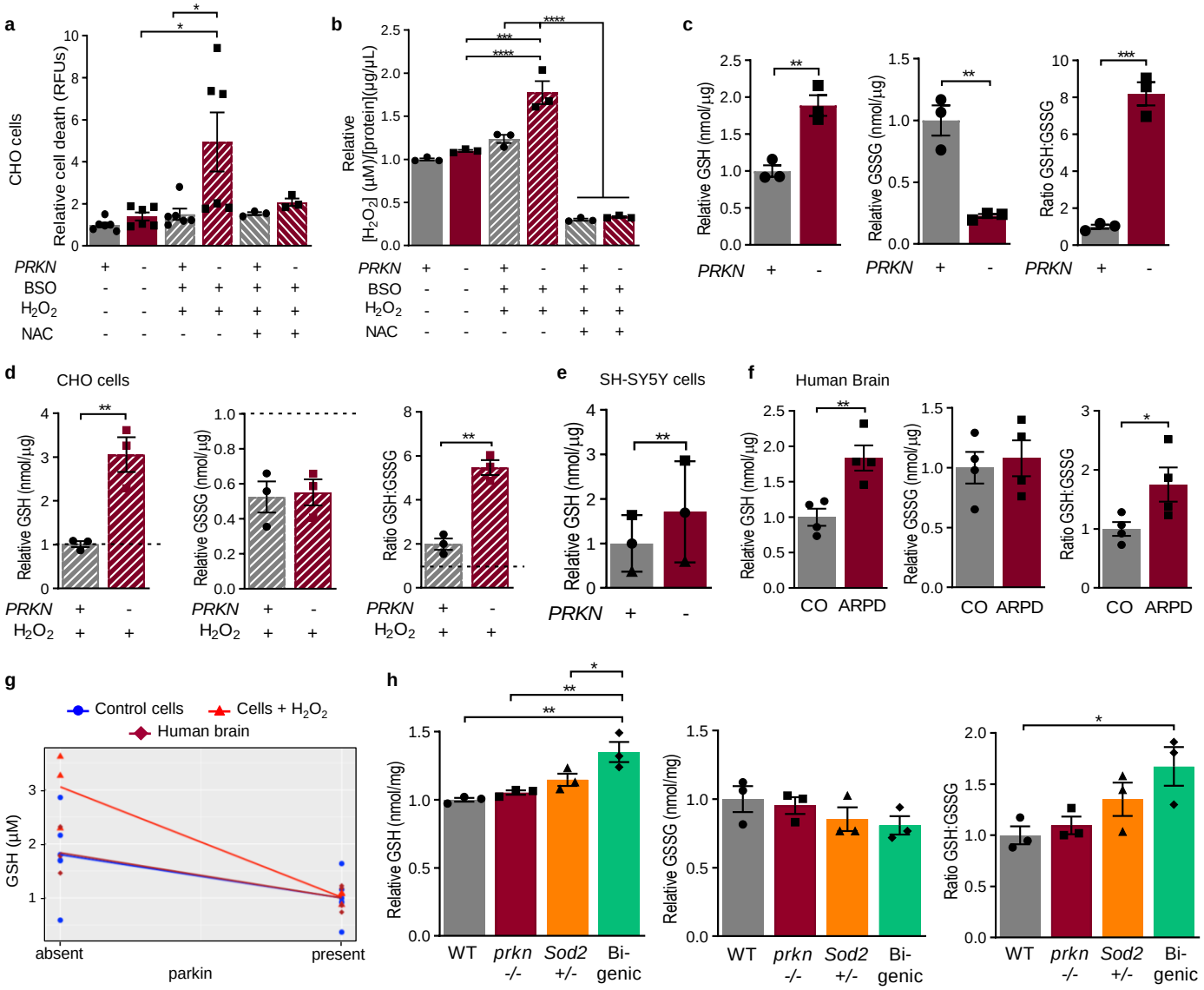

Figure 3: *PRKN* expression alters glutathione metabolism in cells and human brain.
Cellular toxicity **a**, and endogenous H_2O_2 levels **b**, in CHO-parkin and control cells under control or oxidizing conditions (2 mM H_2O_2 + 2mM buthionine sulfoximine (BSO)), with or without supplementation by 20mM n-acetylcysteine (NAC). Reduced GSH, oxidized GSSG, and GSH:GSSG ratio in CHO-parkin or control cells under **c**, control conditions, and **d**, post H_2O_2 stress (HPLC method). **e**, GSH levels in SHSY5Y cells under control conditions (monochlorobimane (MCB) method). Paired data are represented by a distinct symbol. GSH, GSSG, GSH:GSSG ratio in **f**, control and *PRKN* deficient human brain cortices, and **h**, brains of 6 mths-old WT, *prkn* -/-, *sod2* +/- and bi-genic mice (HPLC method). **g**, GSH (µM) levels in several paradigms of *PRKN* genotype comparisons, as indicated. Linear regression lines represented the overall trend of control cells (blue), cells + H_2O_2 (red), and human brain (darker red). A Student t-test or 1-way unpaired or paired ANOVA were used for statistical analysis (* = < 0.05; ** = < 0.01; *** = < 0.001; and ****= <0.0001).

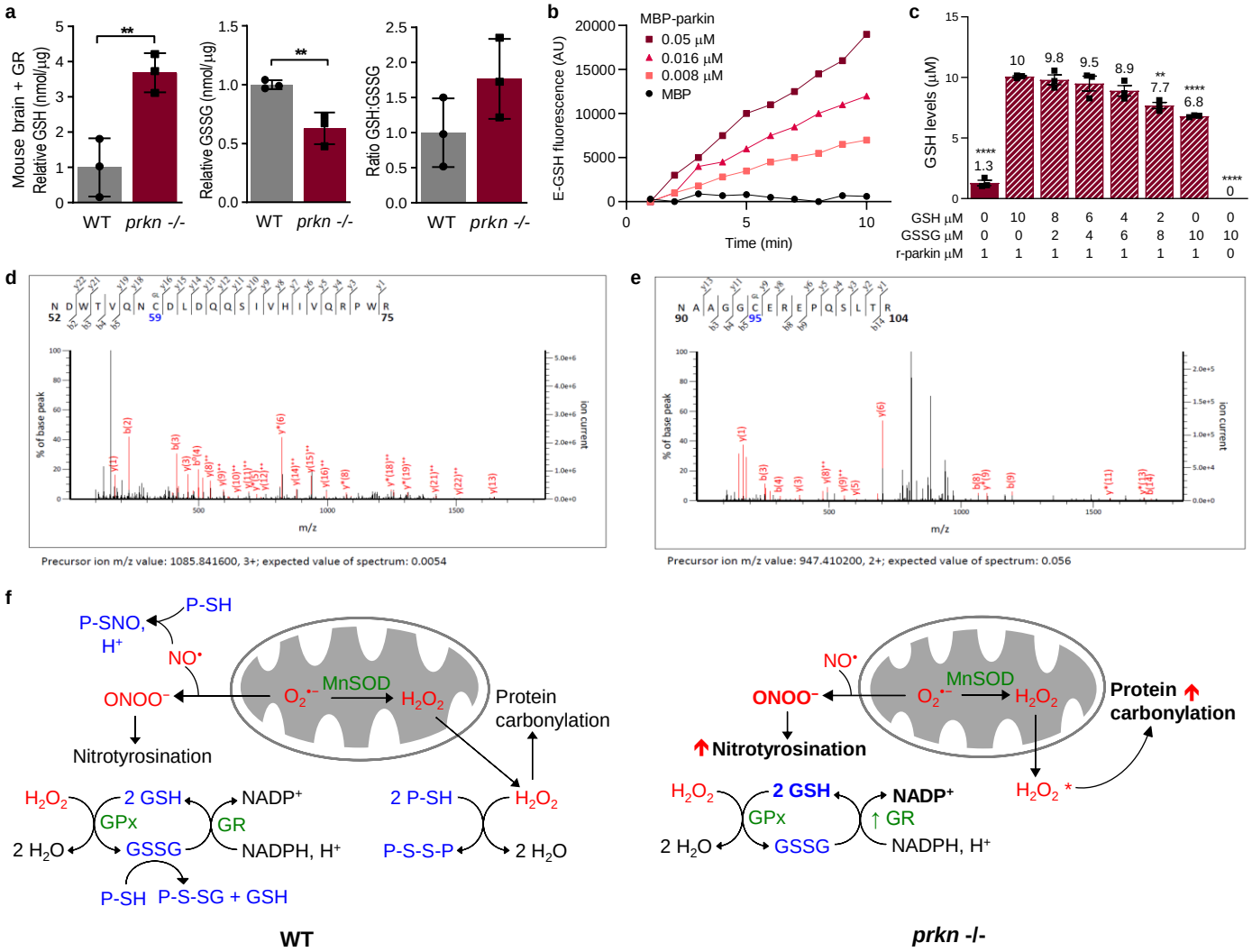

Figure 4: Parkin contributes to glutathione recycling independent of *de novo* synthesis.
a, GSH, GSSG, and GSH:GSSG ratio in 11-13 mths-old WT and *prkn*$^{-/-}$ mouse brains (GR-dependent Tietze method). **b**, E-GSH release after exposure of increasing concentrations of full-length MBP-parkin to 20µM Di-E-GSSG. **c**, GSH levels (µM) of various GSH:GSSG ratios incubated with 1µM of full-length, untagged r-parkin. A Student t-test or 1way ANOVA was used for statistical analysis (** = < 0.01; and *** = < 0.001). **d**, Human parkin peptide aa52-75 is shown, with cysteine 59 S-glutathionylated. **e**, Human parkin peptide aa90-104 is shown, with cysteine 95 S-glutathionylated. **f**, Graphical depiction of redox changes including: GSH recycling; generation of ROS levels (*i.e.*, H_2O_2; superoxide) leading to carbonylation; metabolism of nitric oxide (NO) leading to nitrotyrosination; and function of select enzymes in WT *vs.* parkin-deficient (*prkn*$^{-/-}$) mammalian brain. P, parkin; MnSOD, Mn^{2+}-dependent superoxide dismutase; GPx, glutathione peroxidase; GR, glutathione reductase. * Indicates evidence from human brain[10].

Run	1		2		Mean	
Treatment	Saline (n=1)	MPTP (n=1)	Saline (n=2)	MPTP (n=2)	Saline	MPTP
Number of unique parkin peptides identified	11	18	11	27	11.0	22.5
Number of amino acids identified	106	154	123	323	114.5	238.5
% coverage	23	33	27	70	25.0	51.5
Number of cysteines identified	6	10	7	26	6.5	18.0
% of total cysteines	17.6	29.4	20.6	76.5	19.1	52.9
Number of IAA-modified cysteines identified	6	8	7	22	6.5	15.0
Ratio IAA-cysteines/total cysteines identified	100.0	80.0	100.0	84.6	100.0	82.3
Cysteine -> Dehydroalanine	C195	C195	C195, C240, C252	C195, C237, C240, C252, C376		
Sulfonic acid (Cys trioxidation)	C252	C252	C252, C417, C420	C211, C252		
Sulfinic acid (Cys dioxidation)	n/d	n/d	n/d	C252		
Phosphorylation	n/d	n/d	n/d	S77		
Methionine oxidation	M191, M457	M191, M457	M191, M457	M191, M326, M457		

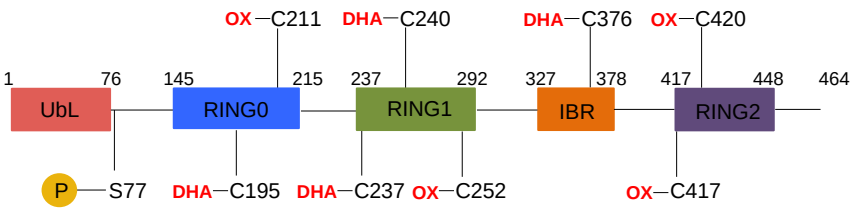

Extended Data Table 1: Parkin cysteines are oxidized in adult mouse brain.
Table summarizing mass spectrometry results highlighting the ratios of the number of IAA-tagged and free cysteines divided by the total number of identified cysteines in wild-type parkin enriched from the brains of mice treated with MPTP (2 independent runs, n=3 brains each) compared to saline controls (2 independent runs, n=3 brains each) under reducing and alkylating conditions (see Methods for details). The means of both runs in each treatment are shown with the ratio (in percent) of IAA-tagged cysteines to total identified cysteines highlighted. Select, oxidative stress-induced, posttranslational modifications found at murine parkin cysteines are highlighted in the table (bottom), *e.g.:* cysteine to dehydroalanine; cysteine dioxidation (=sulfinic acid); and cysteine trioxidation (=sulfonic acid). Phosphorylation and methionine oxidation events (table only) are also listed. Graphic summary of murine parkin domains with selected residues for identified PTMs. OX, oxidized cysteines (sulfinic or sulfonic acid); DHA, dehydroalanine; P, phosphorylation.

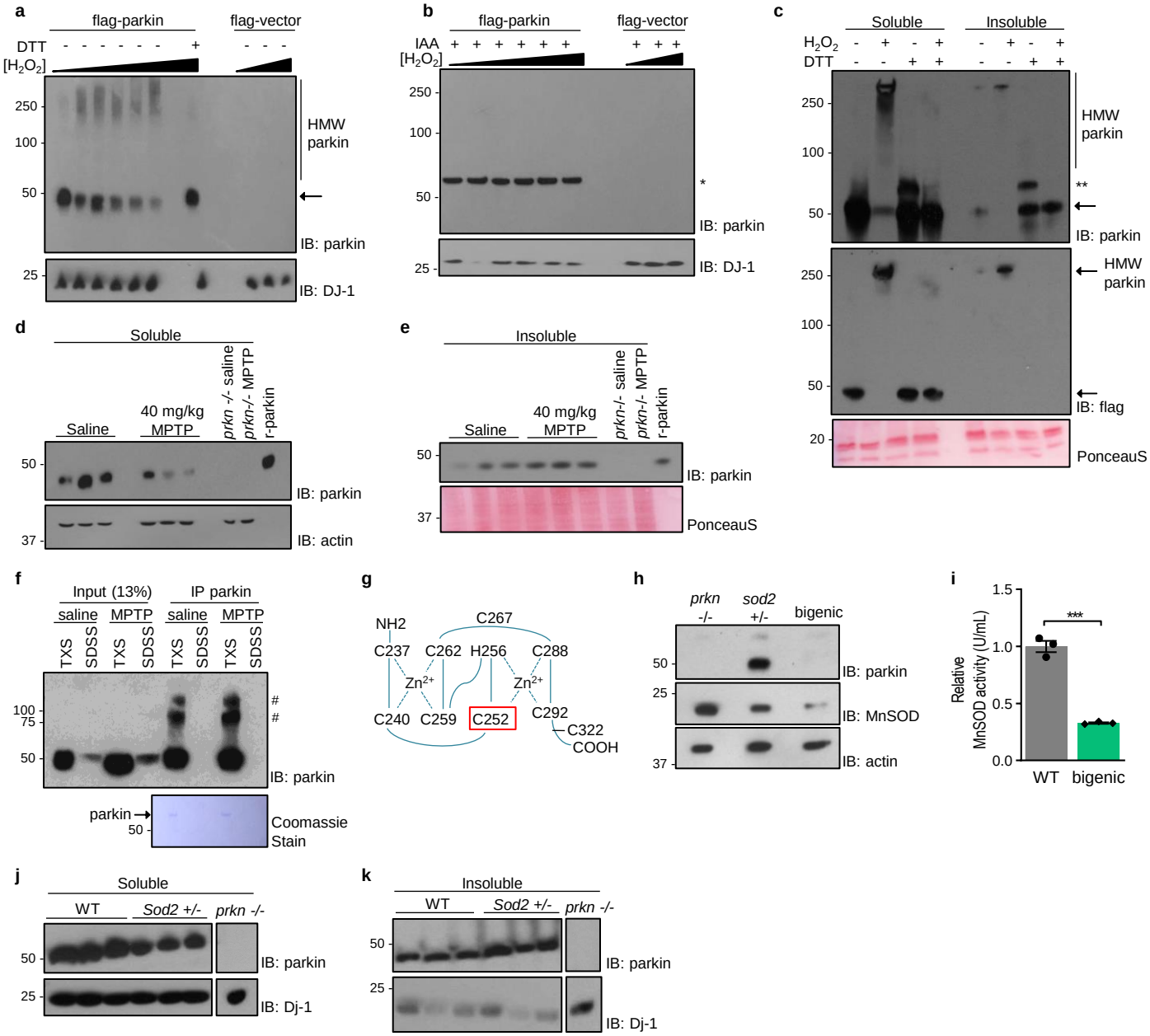

Extended Data Figure 1: Mitochondrial and cytosolic stressors lead to oxidation of cellular parkin promoting its insolubility.

Representative Western blots of parkin and DJ-1 in HEK293-parkin or control cells incubated with increasing concentrations of H_2O_2 (2μM to 20mM) **a**, with the addition of dithiothreitol (DTT) (100mM, 30 mins; lane 8) or **b**, pre-incubating with iodoacetamide (IAA) (10mM, 15 mins). **c**, Representative Western blots of parkin and flag in cell lysates from HEK293-parkin or controls cells under oxidizing and/or reducing conditions. (←) Monomeric parkin, (*) Alkylated-parkin and (**) DTT-modified-parkin. Representative Western blots of parkin distribution in **d**, soluble, and **e**, insoluble fractions of whole or hemi brain homogenates from mice treated with saline or MPTP. **f**, Representative Western blots of immunoprecipitated parkin from mouse brains treated with saline or MPTP. (#) IgG related bands. **g**, Schematic representation of parkin's RING1 domain with the position of an oxidized cysteine residue highlighted (C252). **h**, Representative Western blots of parkin and MnSOD in brains of 2-4 mths-old *prkn*$^{-/-}$, *Sod2*$^{+/-}$ and bi-genic mice. **i**, MnSOD activity in brains of 2-4 mths-old WT and bi-genic mice. Representative Western blots of parkin and Dj-1 distribution in **j**, soluble, and **k**, insoluble fractions of brains from WT and *Sod2*$^{+/-}$ mice. A Student t-test was used for statistical analysis (*** = < 0.001).

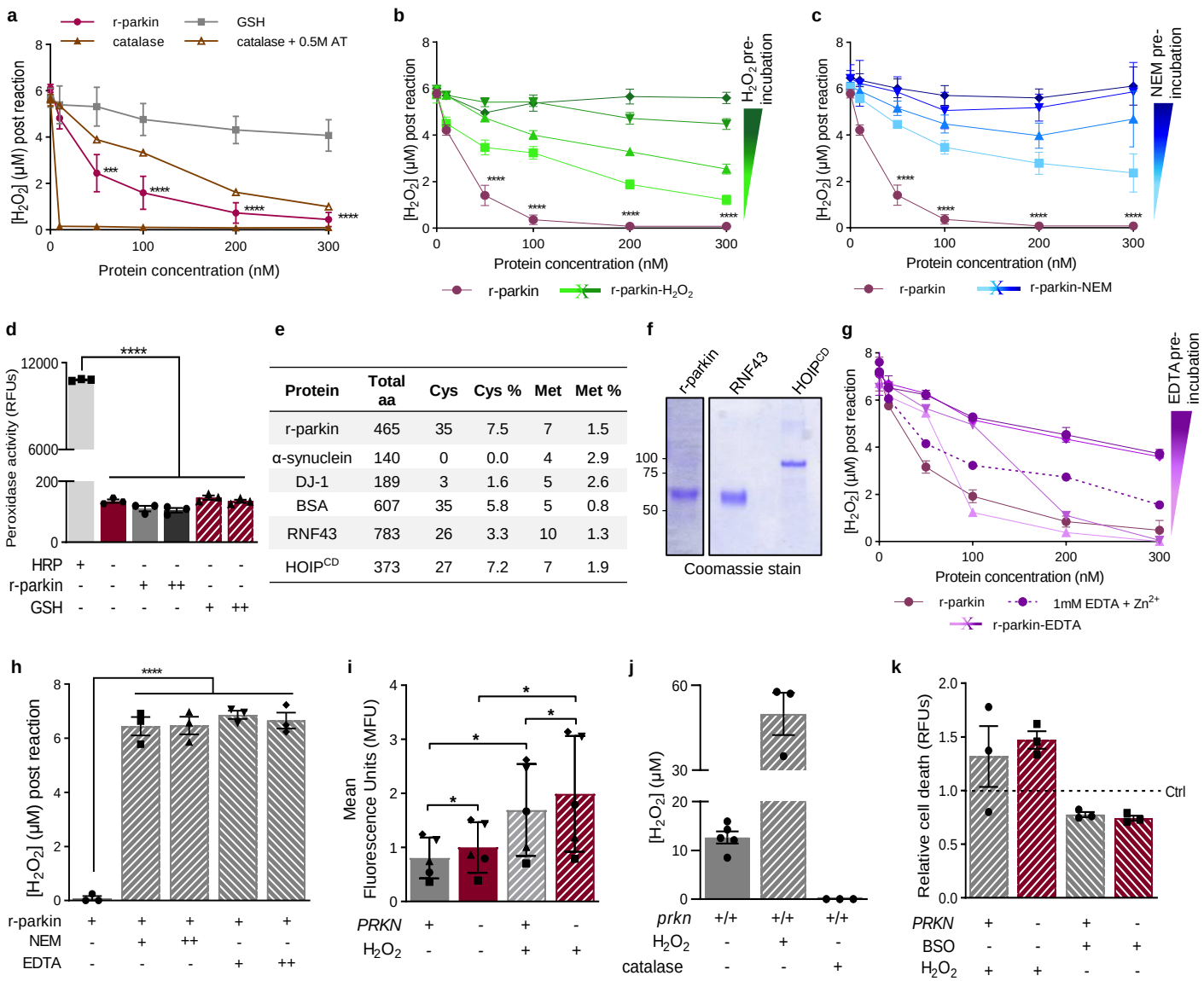

Protein	Total aa	Cys	Cys %	Met	Met %
r-parkin	465	35	7.5	7	1.5
α-synuclein	140	0	0.0	4	2.9
DJ-1	189	3	1.6	5	2.6
BSA	607	35	5.8	5	0.8
RNF43	783	26	3.3	10	1.3
HOIP^{CD}	373	27	7.2	7	1.9

Extended Data Figure 2: Parkin cysteines reduce hydrogen peroxide to lower oxidative stress.
Parkin's reducing capacity **a**, compared to glutathione and catalase, at equal molar concentrations (AT was used to block catalase activity), **b**, post oxidation with increasing concentrations of H_2O_2 (2μM to 2mM), and **c,** after incubation with increasing concentrations of NEM (100μM to 1mM). **d,** Parkin's and glutathione's peroxidase activity in comparison to horseradish peroxidase. **e**, Table summarizing the cysteine and methionine content of parkin, DJ-1, α-synuclein, BSA, RNF43 and HOIP^{cd}. **f**, r-parkin, RNF43 and HOIP^{cd} proteins visualized by Coomassie stain. **g**, Parkin's reducing capacity post incubation with increasing concentrations of ethylenediaminetetraacetic acid (EDTA) (100μM to 1mM). **h**, H_2O_2 reducing capacity for NEM and EDTA. **i**, H_2O_2 levels in live HEK293-parkin or control cells treated with 0 or 2 mM H_2O_2 (flow cytometry). Paired data are represented by a distinct symbol. **j**, AmplexRed assay sensitivity demonstrated by the addition of H_2O_2 or catalase to mouse brain homogenates. **k**, Cell cytotoxicity in CHO-parkin or control cells with the addition of 2mM H_2O_2 or 20mM BSO alone. A 1way, or 2way, unpaired or paired, ANOVA with Bonferroni post hoc analysis were used for statistical analysis (*= <0.05; ** = < 0.01; ***= <0.001; and **** = <0.0001).

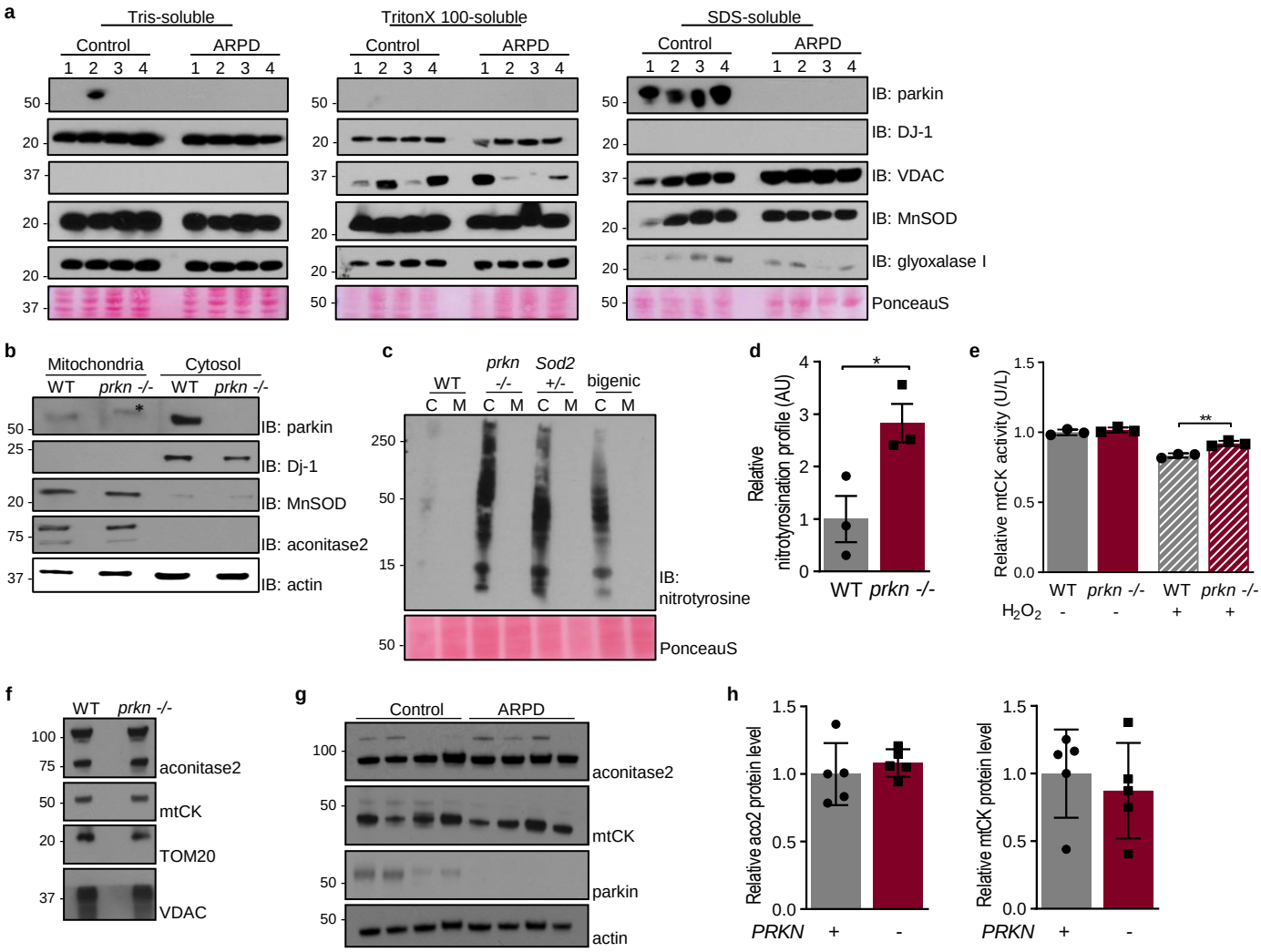

Extended Data Figure 3: *PRKN* expression alters glutathione metabolism in cells and human brain.
a, Representative Western blots of parkin, DJ-1, VDAC, MnSOD, and glyoxalase-1 in Tris-soluble, TritonX 100-soluble and SDS-soluble fractions of aged-matched control and human ARPD (*PRKN* mutant) cortices. **b**, Representative Western blots of parkin, DJ-1, MnSOD, and aconitase-2 in mitochondria-enriched vs. cytosol fractions from WT and *prkn*$^{-/-}$ mouse brains. (*) Non-specific band. **c**, Representative Western blots of nitrotyrosination in heart homogenates from 6 mths-old WT, *prkn*$^{-/-}$, *Sod2*$^{+/-}$ and bi-genic mice. **d**, Quantification of nitrotyrosination signals in WT and *prkn*$^{-/-}$ mouse hearts. **e**, Creatine kinase (mtCK) enzymatic activity in mitochondria isolated from 12 mths-old WT and *prkn*$^{-/-}$ mouse brains. Representative Western blots of aconitase-2, mtCK, TOM20, VDAC and parkin in mitochondrial extracts from **f**, mouse brains, and **g,** human brains. **h**, Quantification of aconitase-2 and mtCK signal distribution in mammalian brains (mouse and human). A Student t-test or 1way ANOVA was used for statistical analysis (* = < 0.05; and ** = < 0.01).

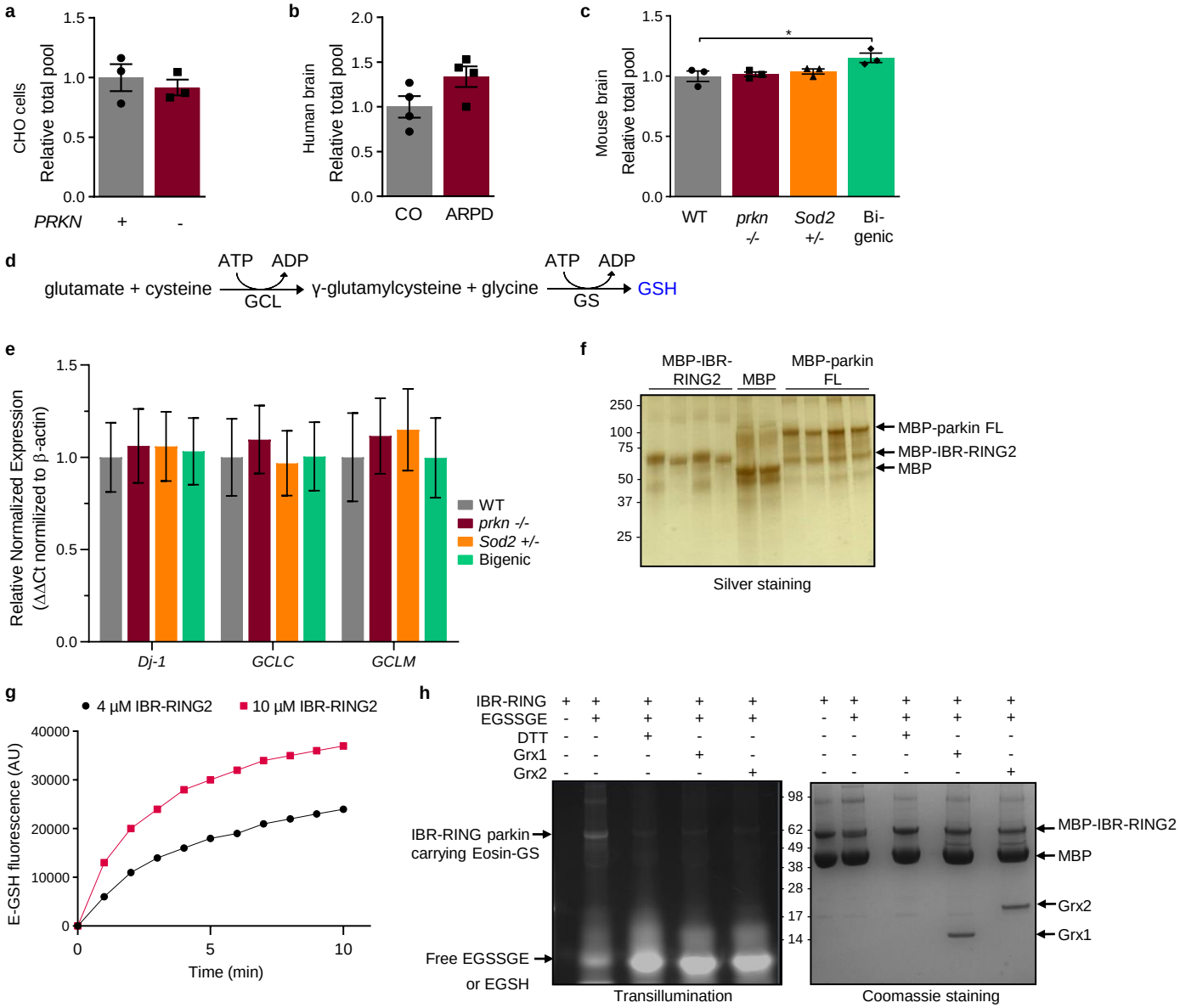

Extended Data Figure 4: Parkin contributes to glutathione recycling independent of *de novo* synthesis

The total GSH + GSSG pool in **a**, CHO cells, **b**, human cortices, and **c**, brain homogenates of 6 mths-old WT, *prkn*$^{-/-}$, *Sod2*$^{+/-}$, and bi-genic mice (HPLC method). A 1way ANOVA was used for statistical analysis (*= <0.05). **d,** Graphic depiction of GSH synthesis from glutamate and cysteine, with glutamate cysteine ligase (GCL) as the rate-limiting enzyme. **e**, *Dj-1*, glutamate cysteine ligase catalytic subunit (*GCLC)* and glutamate cysteine ligase modifier subunit (*GCLM)* gene expression in brains of 6 mths-old WT, *prkn*$^{-/-}$, *Sod2*$^{+/-}$ and bi-genic mice. **f**, Silver stain of MBP-tag (~45-50 kDa), MBP-IBR-RING2 (parkin, aa 327-465, ~60-65 kDa), and MPB-parkin (~90-95 kDa). **g**, E-GSH release post treatment of increasing concentrations of MBP-IBR-RING2 protein with 20μM Di-E-GSSG. **h**, Representative UV transillumination and Coomassie Blue stain gels of S-glutathionylated MBP-IBR-RING2 protein. Results are representative of three independent experiments. Grx1, glutaredoxin-1; Grx2, glutaredoxin-2; EGSSGE, Di-E-GSSG (eosin-labelled oxidized glutathione).